The Brazil Current cyclonic meandering and shelf-slope water exchanges at 27°S-31°S

João Pedro M. de Amorim, Ilson C.A. da Silveira, Milton Borges-Silva, Pedro W.M. Souza-Net, Piero S. Bernardo, Marcelo Dottori, Wellington C. Belo, Renato P. Martin, and Tiago C. Biló

[a]*Oceanographic Institute, University of São Paulo, Praça Oceanográfico, 191, São Paulo, 05508-120, São Paulo, Brazil*

[b]*Centro de Pesquisas, Desenvolvimento e Inovação Leopoldo Américo Miguez de Mello -CENPES/PETROBRAS, Cidade Universitária da Universidade Federal do Rio deJaneiro, Rio de Janeiro, 21941-915, Rio de Janeiro, Brazil*

[c]*Cooperative Institute for Marine and Atmospheric Studies, University of Miami, 4600 Rickenbacker Causeway, Miami, 33149, Florida, United States*

[d]*Atlantic Oceanographic and Meteorological Laboratory, National Oceanic and Atmospheric Administration, 4301 Rickenbacker Causeway, Miami, 33149, Florida, United States*

for publication in

Deep Sea Research Part 1: Oceanographic Research Papers

Highlights

- Observational data were used to describe the velocity structure of two cyclonic meanders near the Cape Santa Marta (28°S).
- LADCP measurements showed the importance of barotropcity on these structures.
- Satellite data shows two spots of eddies generation, one northward and the other southward of the cape.
- CTD casts showed coastal water trapped inside of one meander, and satellite images composites of chlorophyll-a suggest that this is a recurrent phenomenon.

Abstract

The Brazil Current (BC) experiences intense mesoscale activity from its origin on the northeastern Brazilian coast till it reaches the Brazil-Malvinas Confluence. The BC meandering behavior near the Cape Santa Marta (27°S–31°S), has not been well described in the literature. In this study, *in situ* observations and satellite images are used to describe the BC meanders and cyclonic eddies near the cape. The results obtained from two Lowered Acoustic Doppler Current Profilers (LADCP) sections show that these structures are surface intensified but extend through the whole water column. Conductivity Temperature and Depth (CTD) profiles show evidence of coastal water trapping inside an eddy. Altimeter data show two hot spots of cyclones, one at 28.5°S and the other at 30.5°S, with an average of ∼5 and 7 eddies per year, respectively. The eddies generated on both sites have a mean lifetime of 37 days, and no significant differences were found between their surface properties. Satellite images of chlorophyll show that coastal water horizontal advection is a recurrent phenomenon in these eddies, imprinting an eddy stirring signal into their average composites. Furthermore, using Empirical Orthogonal Functions to analyze the BC flow in a mooring line, we observed that the mesoscales meanders are responsible for explaining at least 1/3 of the flow variability in his area.

Key words*:* Brazil Current, cyclonic eddies, mesoscale variability

1. Introduction

The circulation in the western portion of the subtropical South Atlantic Ocean is dominated by a system of western boundary currents. In the upper 500 m there is the Brazil Current (BC), which flows southward along the shelf break and in the outer portions of the continental slope (Stramma and England, 1999; Silveira et al., 2008). At intermediate levels, the bifurcation of a branch of the South Equatorial Current (SSEC) at approximately 28°S (known as Santos Bifurcation, Boebel et al. (1999)) gives rise to the Intermediate Western Boundary Current (IWBC), which flows northward (Luko et al., 2021). South of 28°S, geostrophic computations (Zemba, 1991), lagrangian float trajectories (Boebel et al., 1999) and current meter mooring lines (Müller et al., 1998) show that the BC vertically thickens. This thickening is related to the incorporation of the Antarctic Intermediate Water (AAIW) flow between 500 m and 1500 m of depth, over the continental slope.

From its origin (~15°S) until it reaches the Brazil-Malvinas confluence (~39°S), the BC experiences strong mesoscale activity (Signorini, 1978; Legeckis and Gordon, 1982; Garfield, 1990; Campos et al., 1995; Calado et al., 2008; Soutelino et al., 2011). Some eddies are generated near changes in the shelf orientation due to topographical forcing, as the anticyclones named Royal-Charlotte Eddy (17°S) and the Abrolhos Eddy at 18°S (Soutelino et al., 2011; Arruda and da Silveira, 2019). Also, the vertical shear resulting from the opposite flows of the BC and the IWBC can trigger baroclinic instabilities that evolve until the pinching-off of well-developed eddies, as the cyclones off Cape Frio and Cape São Tomé (Silveira et al., 2008; Mill et al., 2015).

Mesoscale oceanic eddies can drive intense horizontal and vertical motions that affect biological processes. According to McGillicuddy (2016), there are several mechanisms by which these features can affect marine biological processes, for example: the vertical uplift of the upper thermocline, lateral advection of nutrients and trapping water in its interior and eddy induced Ekman pumping due to variations in wind stress. Pascual et al. (2015) shows that the vertical velocity induced by mesoscale eddies alone can sustain the observed levels of net primary production in the vicinity of the Gulf Stream (GS). Also, eddies can be generated in the shoreward edge of western boundary currents and directly affect biological production. During their formation and propagation, these eddies may be constrained between the coast and the current jet, impinging on the continental shelves and entraining the shelf waters (Everett et al. 2015). On the Eastern Australian Current (EAC), the eddies generated by the current can be an important source of water exchanges between the shelf and slope (Ismail and Ribbe, 2019; Roughan et al., 2017; Malan et al., 2023). In the Kuroshio extension, temporal and spatial changes on nutrient and chlorophyll distributions are associated with frontal meanders generated by the current (Kimura et al. 1997; Kimura et al. 2000).

Along the southeastern Brazilian coast, vortical structures generated by the BC can be a relevant source of cross-shelf exchanges and promote the extrusions of nutrients-rich waters offshore on the Southeastern Brazilian coast (Campos et al., 2000; Calado et al., 2010). Calado et al. (2010) showed that coastal and oceanic systems interact due to the BC and its cyclonic meanders. The authors show that this interaction can cause (or enhance) coastal upwelling, where coastal waters encircle the BC cyclonic meanders and are ejected offshore as it grows. Palóczy et al. (2014) quantified the importance of the BC and the unstable meander baroclinic adjustment on supporting the Ekman dynamics causing coastal upwelling near Cape São Tomé. They found that the upwelling events with meanders tend to receive less impulse from the wind and tend to be more intense. Arruda and da Silveira (2019) analyzed the role of interactions between Abrolhos Eddy and Vitória Eddy in ejecting upwelled waters offshore at the surface. According to the authors this dipole is able to promote the upwelling of upper pycnocline waters near the shelf-break and the BC acquires a cross-isobath direction, transporting these waters offshore.

The southern Brazilian coast is predominantly characterized by changes in shelf orientation. The Cape Santa Marta (CSM), located between 27°S-28°S, marks the transition area between the Santos and Pelotas sedimentary basins. The coast follows an N-S orientation north of CSM, while farther south, it is oriented NE-SW. The shelf circulation in this area is driven by seasonally reversing winds (Castro and Miranda, 1998; Palma et al., 2008), which have a substantial imprint on the local water mass distribution due to their influence on the La Plata River plume and on upwelling events (Campos et al., 2013; Piola et al., 2018). Additionally, near the shelf break at the vicinities of the CSM, BC cyclonic meanders and eddies with approximately 100 km of diameter have been reported through sea surface

temperature (SST) satellite images as recurrent features related to vorticity waves which propagate their phase downstream (Garfeld, 1990; Campos et al., 1995). Despite the 90's studies and the relative recent attention BC meanders and eddies have received north of 28°S (Rocha and Simoes-Sousa, 2022; Uchoa et al., 2023), the BC structure and its mesoscale activity off southern Brazilian coast have been almost unexplored. Therefore, basic characteristics of BC's mesoscale variability and their role in shelf-slope exchanges remain largely unknown.

In this paper, we provide the first description and characteristics of the BC cyclonic meanders near 28°S as well as observational evidence of its role in shelf-slope exchanges. To do so, we used two quasi-synoptic data sets, an array of moored current meters, and satellite imagery to describe the top bottom BC's velocity patterns and its associated water masses distribution near CSM. This paper is organized as follows: section 2 describes the data and methods employed in this effort; section 3 describes the observed structure of two CSM cyclonic meanders; in section 4, we examine the cyclones variability using satellite-derived products and moored instruments; in section 5, we analyze the cyclones signature on chlorophyll fields; in section 6, we present the conclusions of this study.

2. Materials and Methods

2.1 In-situ observations

Two *in-situ* observational datasets from distinct oceanographic cruises and one historical moorings line are used in this study. The quasi-synoptic data sets are employed to describe the vertical and horizontal structures of the meanders while the moorings lines are used to analyze the BC flow variability.

The first quasi-synoptic dataset is composed of three transects of oceanographic stations obtained in November of 2013 (11/18-11/23). The data are part of the CERESV Experiment, which aimed to study carbon fluxes in the Brazilian continental margin (Figure 1). During the CERESV cruise, vertical profiling was taken using Conductivity, Temperature and Depth (CTD), Lowered Acoustic Doppler Current Profiler (LADCP), vessel-mounted Acoustic Doppler Current Profiler (VMADCP) as well as Niskin bottle water samples.

The second quasi-synoptic data set consists of 12 CTD-LADCP stations and VMADCP profiles obtained in November of 2003 (11/07 - 11/11) during the MR03- K04 Leg 4 cruise (hereafter MR03) from the World Ocean Circulation Experiment (WOCE). The mooring transect used in this work is composed of the BW333, BM334, BE335, and W906 mooring lines, which are also from WOCE (Müller et al., 1998; Hogg et al., 1999). They are equipped with conventional rotary current meters and ADCPs. For these data, gap periods were filled in using the empirical orthogonal functions (EOF) of the velocity anomaly time series (Beckers and Rixen, 2003; Rocha et al., 2014).

During both surveys, the CTD downcast data were spike-removed, averaged into a 1- m bin, and smoothed using a 21-point Hanning filter to remove high-frequency variations. We used the GibbsSeaWater (GSW) Oceanographic Toolbox of the Thermodynamic Equation of SeaWater TEOS-10 (McDougall and Barker, 2011) and the neutral density package (Jackett and McDougall, 1997) to compute the recommended hydrological variables. Also, nutrient concentrations (silicate, phosphate, ammonium, nitrate, nitrite, and chlorophyll-a) were obtained from the water samples collected at CERESV cruise. These samples were analyzed following the procedures described by Grasshoff et al. (2009).

Top-bottom velocity profiles were obtained in both cruises using a downward-looking 300 kHz LADCP from RD Instruments. These data were processed following the procedures described by Fischer and Visbeck (1993) and Visbeck (2002). Additionally, 75 kHz VMADCP measurements taken along the ship's route were processed using the software Common Ocean Data Access System (CODAS) from the Currents Group of the University of Hawaii.

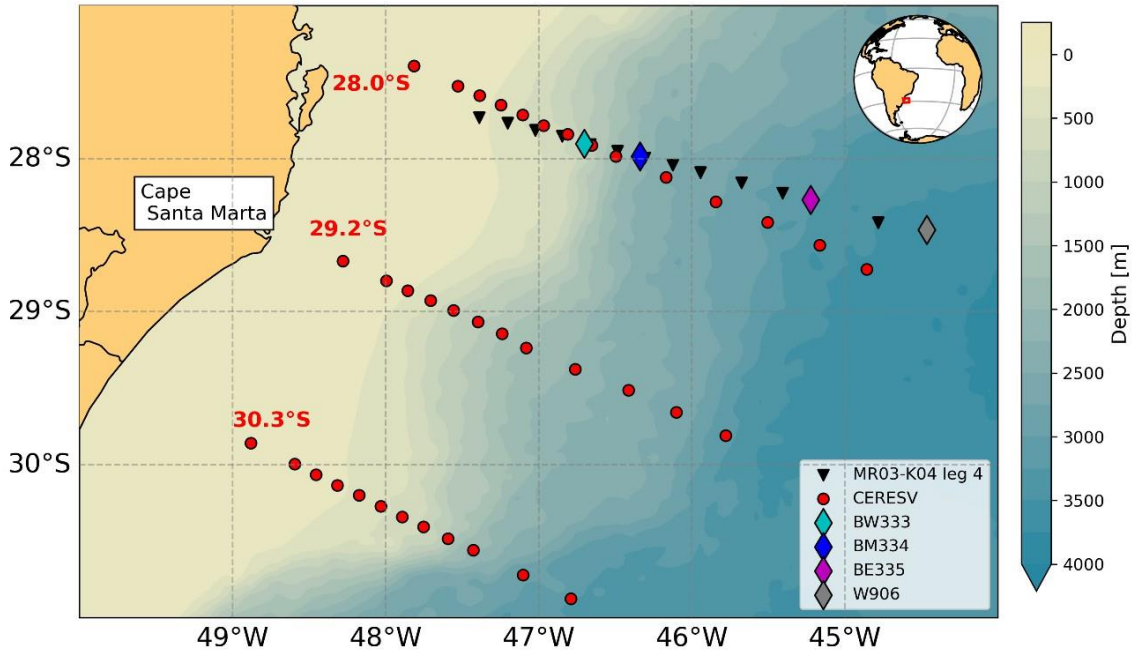

Figure 1: The data set of *in-situ* observations explored in this study: circles (triangles) represent the locations of the CTD-LADCP stations of the CERESV (MR03-K04 Leg 4) cruise and the diamonds represent the positions of the mooring lines, the large red numbers are the transects identification and correspond to their respective mean latitudes.

To interpolate the velocity measurements between the vertical levels and to vertically extrapolate the resulting profiles towards the bottom, we applied a vertical six dynamics mode fitting following the guidelines of Wunsch (1997) and Szuts et al. (2012) in the LADCP data of MR03 cruise and on the WOCE moorings. This fitting is done by considering that the horizontal velocity vector can be described as:

$$u\,(x, y, z, t) \;=\; U_i(x, y, t)\; F_i(z), \tag{1}$$

where *Ui* are the amplitudes of the i-th vertical mode and *F* is the i-th vertical mode associated. The vertical modes *F* are calculated numerically by solving the eigenvalues equation:

$$\frac{d}{dz}\,\frac{1}{N^2}\,\frac{dF_i}{dz} + \lambda_i F_i = 0, \tag{2}$$

where N^2 is the buoyancy frequency and λi the eigenvalues. The boundary conditions for *Fi* is flat bottom and rigid lid, given by:

$$\frac{dF_i}{dz} = 0, z = (-H, 0), \tag{3}$$

each vertical mode obtained is vertically orthogonal to one another and is normalized to have unit magnitude when projected onto itself. Then, the velocity structure can be recovered following the sum of all vertical modes, defined as:

$$u(x, y, z, t) = \sum_{i=1}^{\infty} U_1(x, y, t) F_i(z). \tag{4}$$

For the LADCP data, we used the N^2 profiles obtained on the CTD-casts while for WOCE mooring line we used the climatological N^2 profiles obtained from World Ocean Atlas (Boyer et al., 2018). The latter approach proved to perform well in obtaining full top-bottom profiles where observations only at a few vertical levels were available in the BC domain (Biló et al., 2014; Rocha et al., 2014; Amorim et al., 2023).

Finally, both VMADCP and LADCP measurements from all three CERESV transects were used to map the horizontal flow patterns at different vertical levels following the method developed by Li et al. (2006). This method proposes an algorithm for the computation of stream function and velocity potential from given horizontal velocity vectors by solving a minimization problem, which is applicable to irregular domains such as bordered oceans.

2.2 Satellite data

Absolute Dynamic Topography (ADT) Level 4 product and derived geostrophic currents and anomalies were employed in this study to analyze surface circulation patterns. This product spans from January 1993 to the present and is distributed by Copernicus Marine Environment Monitoring Service (CMEMS). We also analyzed the Mesoscale Eddy Trajectories Atlas multi satellite delayed-time product (META3.2exp) produced by SSALTO/DUACS and distributed by AVISO with support from CNES, in collaboration with IMEDEA (Pegliasco et al., 2022). The META3.2exp employs the eddy detection method developed by Mason et al. (2014) applied to altimetry data.

This product provides specific characteristics for the tracked eddies, such as the amplitude, center position, radius, and average swirling speed. We obtained the growth rates from the detected eddies by taking $\sigma = d/dt\ ln$(radius) similarly to Silveira et al. (2023) and phase speeds estimates were obtained from the distance between consecutive detections of eddy center position. We removed from our analyses all eddies generated over the continental shelf (~150 m), where higher errors are expected due to tidal correction (Silveira et al., 2023), and eddies with lifetimes inferior to 10 days.

To analyze the surface winds circulation during the cruises we used daily wind data from the NOAA/NCDC Blended Seawinds L4 product (Zhang et al., 2006) available in http://www.ncdc.noaa.gov, which is a gridded and blended sea surface winds product from multiple satellites measurements to resolve multi-temporal and spatial scales phenomenon.

We constructed composite averages of chlorophyll-a (Chl-a) spatial anomalies in eddy-centric coordinates. For that, we used the Chlorophyll Type 1 product from the Global Ocean

Colour for Carbon Cycle Research-GlobColour (Lavender et al., 2009). The GlobColour product spans from September 1997 to the present with a horizontal resolution of 0.04° and results from merging the measurements from several Chl-a sensors. First, we constructed log-transformed 7-day averages of Chl-a with the GlobColour data set for the period of 1998 to 2019. Then, we determined spatial anomalies (Chl-a') by computing a moving spatial average of 333 x 333 km (3° x 3°) on the log[Chl-a] fields and then subtracted these fields from the original 7-day averages similarly to Luko et al. (2022). For each eddy event, we used the core position and effective radius (ER), which is the radius of the best circle fitting the eddy SSH contour, both variables are from the META3.2exp (see the previous paragraph) and then interpolated the Chl-a' to an area of 2 x 2 ER centered on the eddy core. Cloud coverage is a frequent issue in this region and represents a limitation on Chl-a images (Saraceno and Provost, 2012). Therefore, for each eddy, we selected only images where at least 80% of its area was filled with valid data. This approach resulted in a total of 1414 valid eddy- centric images.

3. The Vertical and Horizontal Structures of Brazil Current Meanders

In this section, we describe the observed meander structures using the *in-situ* measurements. First, we provide a description of the vertical patterns of the features and their water masses composition. After that, we provide observational evidence that the meander observed during CERESV plays a key role in coastal water exchanges with the open ocean.

3.1 Velocity patterns and water masses

During both cruises, the scattered TS diagram (Figure 2a) shows that the hydrographic structure contains the water masses typically found in Figure 2a the Southwestern Atlantic. Tropical Water (TW) is located in the upper layers, with salinity and temperature values greater than 36 g kg^{-1} and 20°C, respectively. Below this layer, the South Atlantic Central Water (SACW) is characterized by an almost straight distribution on the TS diagram (reference). The salinity minimum is observed in the intermediate layers, indicating the presence of the Antarctic Intermediate Water (AAIW). At depths greater than ~1200 m, Upper Circumpolar Deep Water (UCDW) is found, marked by an increase in salinity. North Atlantic Deep Water (NADW) is the main water mass found at depths greater than ~1700 m, although some profiles also show the presence of Lower Circumpolar Deep Water (LCDW). Additionally, it is interesting to note that the CERESV cruise contains surface waters with salinities < 36 g kg^{-1} and temperatures above 20°C, which according to Piola et al. (2000) results from the mixing between TW and the continental runoff, known as the Subtropical Shelf Water (STSW) in our study area.

Figures 2b and 2c illustrate the cross-sectional velocity fields for the MR03 and CERESV cruises, respectively. Therefore, positive (negative) velocities are considered to the northeast (southwestward) along the slope. Figure 2b depicts the meander from MR03 cruise, where the coastal lobe presents velocities lower than 0.10 m s^{-1} over the upper slope near the shelf break. The northeastward velocity signal is horizontally limited by stations 624 and 627, delimiting a horizontal and vertical extent of approximately 55 km, and 1250 m, respectively. Further offshore, the whole water column (from surface to 2500 m) between stations 628 and 632 (110-202 km) flows southwestward. We observe that this oceanic lobe has a distinguishable velocity core with maximum velocities of -0.60 m s^{-1} at the surface (station 630). The coastal lobe from the CERESV cruise presented in Figure 2c shows a well-defined

velocity signal from the surface to 1000 m depth between stations 130 and 128 (width ~40 km). Moreover, it has one velocity core with maximum velocities of 0.12 m s^{-1} at a depth of approximately 130 m. The oceanic lobe (stations 127 and 124) from the meander of CERESV cruise has a prominent velocity core with subsurface velocities of approximately 0.37 m s^{-1}.

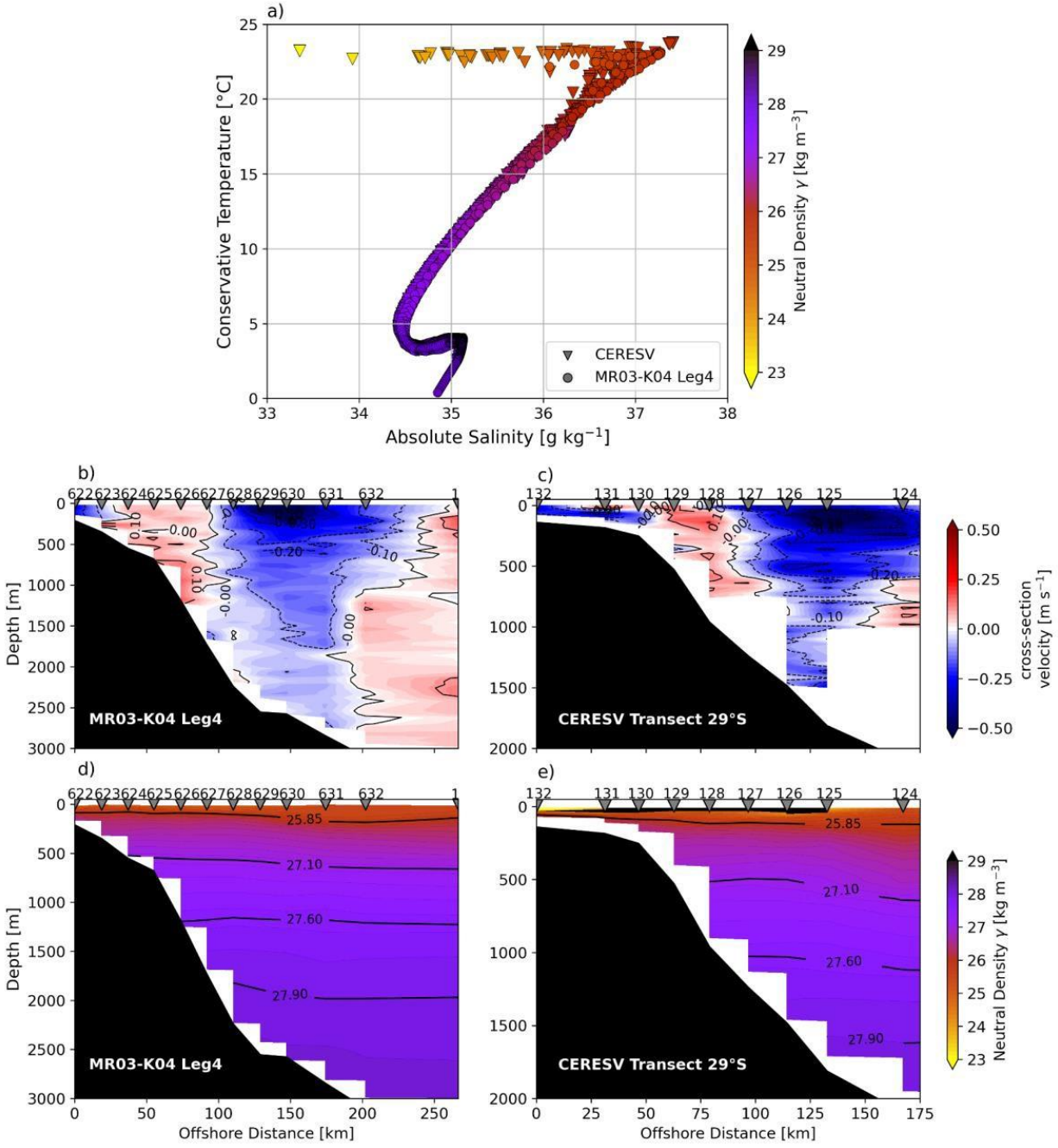

Figure 2: (a) Scattered TS diagram colored with neutral density values during CERESV and MR03 cruises. Cross-sectional velocities and neutral density distributions observed during the MR03 (b,d) and CERESV (c,e) cruises, respectively. The gray triangles indicate the positions of the CTD and LADCP stations. The black contours on (d) and (e) denote the water mass interfaces following Valla et al. (2018) and Silveira et al. (2022), the color scheme was masked for the regions where the STSW was found with a black mask on (e). Note that the limits of the transect panels axes are different for better visualization.

By combining the velocity pattern with the sectional distribution of the water mass neutral density interfaces (Figure 2d-e) from Valla et al. (2018) and Silveira et al. (2022), we are able to associate the flow direction of each water mass during the cruises. The total amount of water that is crossing the MR03 transect in the coastal lobe is approximately 2.0 Sv (1 Sv = 10^6 m^3 s^{-1}), which is composed of TW (γ < 25.85 kg m^{-3}), SACW (25.85 kg m^{-3} < γ < 27.10 kg m^{-3}) and a portion of AAIW (27.10 kg m^{-3} < γ < 27.60 kg m^{-3}). Its oceanic lobe transports TW and SACW in the upper 500 m, AAIW at ~500-1200 m, UCDW (27.60 kg m^{-3} < γ < 27.90 kg m^{-3}) at approximately 1200-1500 m, and NADW (27.90 kg m^{-3} < γ < 28.10 kg m^{-3}) near the bottom at depths greater than 1500 m. Excluding the NADW of the volume transport computation, the MR03 oceanic lobe transports approximately -22.7 Sv, which is comparable to the -22.8 Sv estimated by Zemba (1991) at 31°S from geostrophy. If we incorporate the NADW flow into the volume transport it becomes approximately -26 Sv, which is 1.3 Sv greater than the -24.7 Sv from Zemba (1991) estimate. Considering the meander from the CERESV cruise, its coastal lobe has a transport of approximately 1.5 Sv, composed of TW, SACW and a fraction of AAIW. The oceanic lobe transports -14.5 Sv (excluding the NADW). This suggests that 13 Sv should be crossing the 29.2°S transect poleward.

Although the observed meanders have differences in their velocity structure, the general water mass circulation pattern is very similar among them. From our velocity analysis, it is clear that the vortical structures presented in Figure 2 are meanders, in which the oceanic lobe presents BC jet flowing south-southwestward. The Cape Santa Marta meanders recirculate about 1.5-2 Sv according to our estimates.

The vertical mode fitting (Eq. 4) for the MR03 LADCP data (Figures 3a-3c) reveals the importance of barotropicity on the meander structure. Barotropic velocity estimates explain approximately 36% of the observed feld variance, with maximum absolute values of -0.25 m s^{-1} on station 630. Adding the first baroclinic mode, nearly 70% of the variance of the observed velocity field is explained, including the surface intensification observed on the off shore lobe of the MR03 meander. The mode fitting for 6 LADCP stations obtained inside the CERESV eddy also show similar results (Figures 3d-3f), where barotropic mode explained 34% of the variance and along with the first baroclinic mode 63%.

3.2. Evidence of shelf-slope mass exchanges and water trapping

In an attempt to expand our previous description of the observed cyclonic meander on CERESV cruise, we obtained the stream function (ψ) following the procedures of Li et al. (2006). In Figure 4 we present the ψ field at the surface (obtained from altimeter), at 30 m and at 700 m from the CERESV cruise. Both surface and 30 m maps show that the transect 29.02°S does not cross the center of the eddy structure, which seems to be located a little south (center of maximum ψ). According to META3.2exp, this cyclonic meander had an average radius of 54 km, which agrees with the estimated diameter of more than 100 km observed on the sectional velocity distribution (Figure 2c).

The STSW previously depicted on TS diagram (Figure 2a) seems to extend more than 120 km away from the 150 m isobath, based on the linearly interpolated salinity fields (see the 36 g kg^{-1} isohaline in Figures 4d-f). The 36 g kg^{-1} isohaline at 5 m (Figure 4a and 4d) follows the external edge of the oceanic lobe, corroborating the ψ mapping and indicating that the observed low salinity distribution may be associated with the meander circulation. Matano et al. (2014) performed a series of numerical simulations that showed the vicinity of 28°S as a

spot of shelf-open ocean mass exchange. Based on their results, the authors argued that the exportation of the shelf waters to the open ocean is strongly associated with the BC mesoscale activity. Our current dataset limits the ability to estimate the amount of shelf waters (S < 36 g kg^{-1}) being exported by the cyclone. Thus, we assume that the linearly interpolated salinity fields reasonably represent the synoptic pattern of salinity. We combine this with the interpolated velocity field at each 10 m depth (from 10 m to 100 m), following the guidelines of Li et al. (2006). Therefore, the offshore eddy-driven transport of shelf waters crossing the 1000 m isobath was ~0.4 Sv, and the volume of freshwater away from the 150 m isobath was about 93 x 10^{10} m^3.

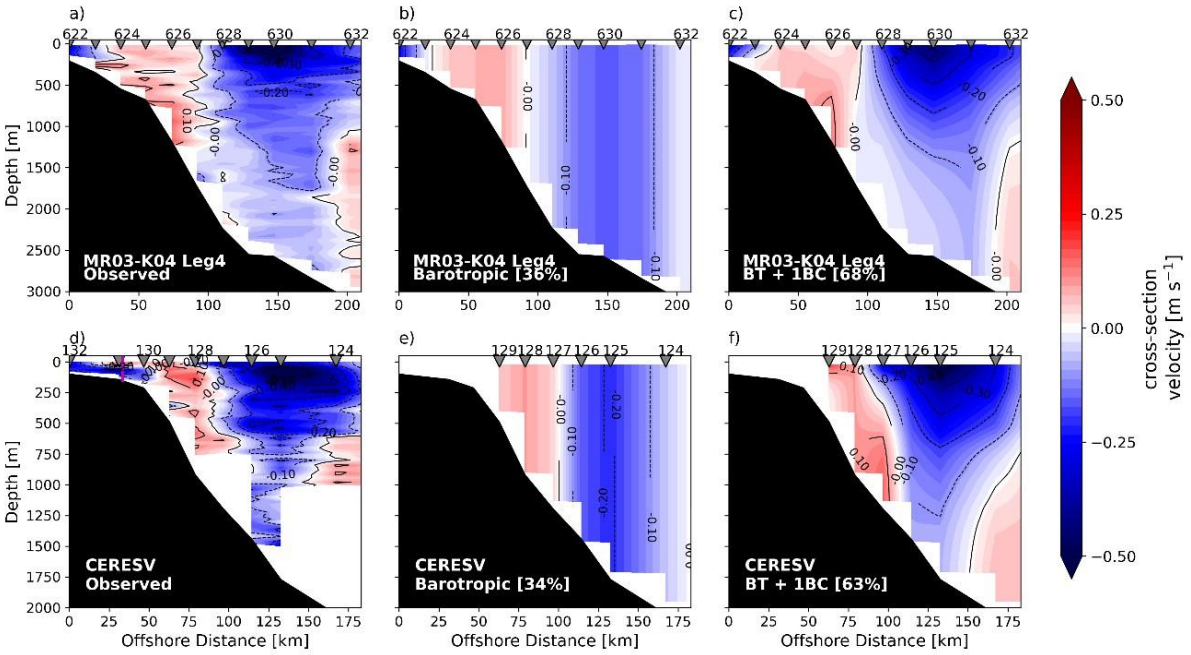

Figure 3: Modal projection into the observed velocity field: a) Observed cross-section velocity for MR03 data; b) barotropic mode projection; c) barotropic +1st baroclinic mode projection. d) to (f) are similar to (a) - (c) but for the CERESV cruise. The percentages represent the explained variance of the used modes. Vertical magenta line on (d) denotes the 150 m isobath.

This low salinity tongue (i.e, shelf waters) crosses the shelf break and reaches the 2000 m isobath way past the continental shelf break (Figure 4). We observe that station 126 is the only location where the STSW penetrates at depths of ~55 m (Figure 4f), suggesting a downwelling of surface waters near the center of the cyclonic feature (Figure 4f).

As suggested by the temperature and salinity distribution in the TS space (Figure 2a), the STSW entrainment signal inside the meander is only visible in the salinity distribution (Figures 5a and 5b). Temperature variations near the surface (≤ 1.5°C) (Figures 5c and 5d) are very small compared to salinity variations in all CTD stations. Note that the BC cyclones near Cape Santa Marta were originally reported from SST satellite imagery by Campos et al. (1995). However, we point out that surface temperature may not always be a good tracer for detecting these cyclones due to the lack of thermal contrast between shelf and BC waters (Figure 5d).

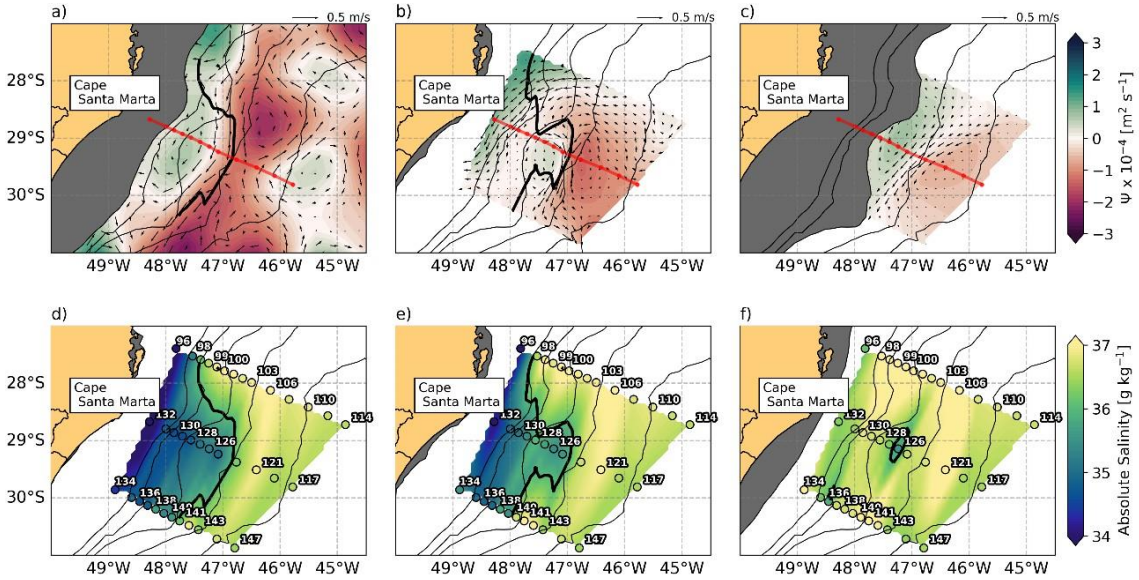

Figure 4: Altimeter derived stream function (ψ) and velocity vectors at the surface (a), mapped stream function and velocity vectors following Li et al. (2006) at 30 m (b) and 700 m (c) depth. Linearly interpolated horizontal salinity distributions at 5 m (d), 30 m (e) and 55 m depth (f). The thick black line denotes the *in situ* 36 g kg^{-1} salinity line at 5 m (a,d) and 30 m depth (b,e), respectively. The gray mask covers areas shallower than 150 m (a), 10 m (d), 30 m (b,e), 700 m (c), and 70 m (f). The thin black contours are the 150 m, 200 m, 700 m, 2000 m and 3000 m isobaths. The red line on a-c refers to the transect of Figures 2c,e and Figures 3d-f.

Due to this salinity contrast, the stratification in the upper 100 m approximately is mainly salinity-dominated (Figures 2 and 5). While the isopycnals in the upper layer are arched upward, as one should expect from a low-pressure feature, the isopycnals are configured downward in the upper 100 m at the eddy center. This isopycnal pattern is characteristic of a cyclone under the influx of the Ekman dynamics. This phenomenon has been called the eddy wind effect by Flierl and McGillicuddy (2002) and McGillicuddy Jr (2015). Under this effect, the upper boundary layer induces convergence on the top of the meander. Indeed, water is trapped in the center of the cyclonic eddy and the surface waters tend to be pushed downward in the water column due to Ekman downwelling (Callbeck et al., 2017), in agreement with the presence of low salinity waters at 55 m on station 126 (Figure 4f).

Therefore, an important process to be verified is the influence of the wind over the shelf-slope mass exchange. It is well known that the wind is the primary forcing agent of the circulation in the southern portion of the Brazilian continental shelf (Castro and Miranda, 1998). Additionally, the northeasterly winds play an important role in the exportation of surface shelf waters to the open ocean and in the shelf-break upwelling system (Campos et al., 2000; Castelao et al., 2004; Palma et al., 2008; Matano et al., 2010). Thus, we carried out a simple assessment of the Ekman transport based on 9 days of sea surface winds.

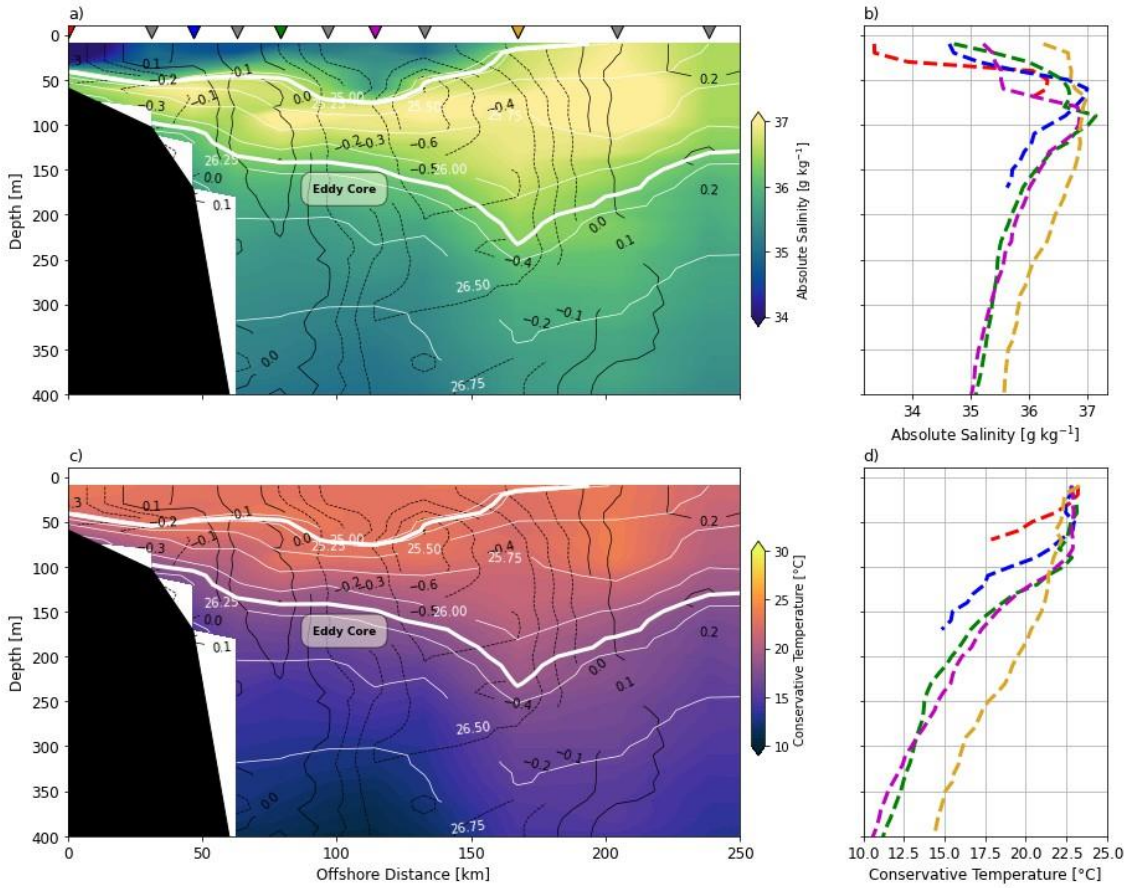

Figure 5: Vertical sections of salinity (a) and temperature (c) on the upper 400 m from transect 29.2°S where the STSW is present and selected salinity and temperature profiles (b and d, respectively). Black and white lines on (a) and (c) are the velocity and neutral density contours, respectively. Colored lines on (b) and (d) are selected according to the position of the profiles on the colored triangles in (a).

Figure 6 shows the sea surface winds vectors and magnitude from 5 days before the start of the CERESV cruise to the end of the transect that crossed the meander (November 13, 2013 to November 21, 2013). Between 11/13 and 11/17, there are two shifts in the direction of the winds, probably associated with cold fronts that are common in this region (Stech and Lorenzzetti, 1992; Rodrigues et al., 2004). During the cruise period (11/18-11/20), we observed intense and persistent northeasterly sea surface winds (>10 m s^{-1}). The approximate duration of 72 h of such winds is enough to allow the development of an offshore Ekman transport at the surface since the inertial period (T*i*) is around 25.5 h. Additionally, this wind configuration blowing over the meander is consistent with the eddy-wind effect proposed previously in this work. As a result, the STSW distribution during CERESV is likely explained by the combined effects of the northeasterly winds blowing over a BC cyclonic meander.

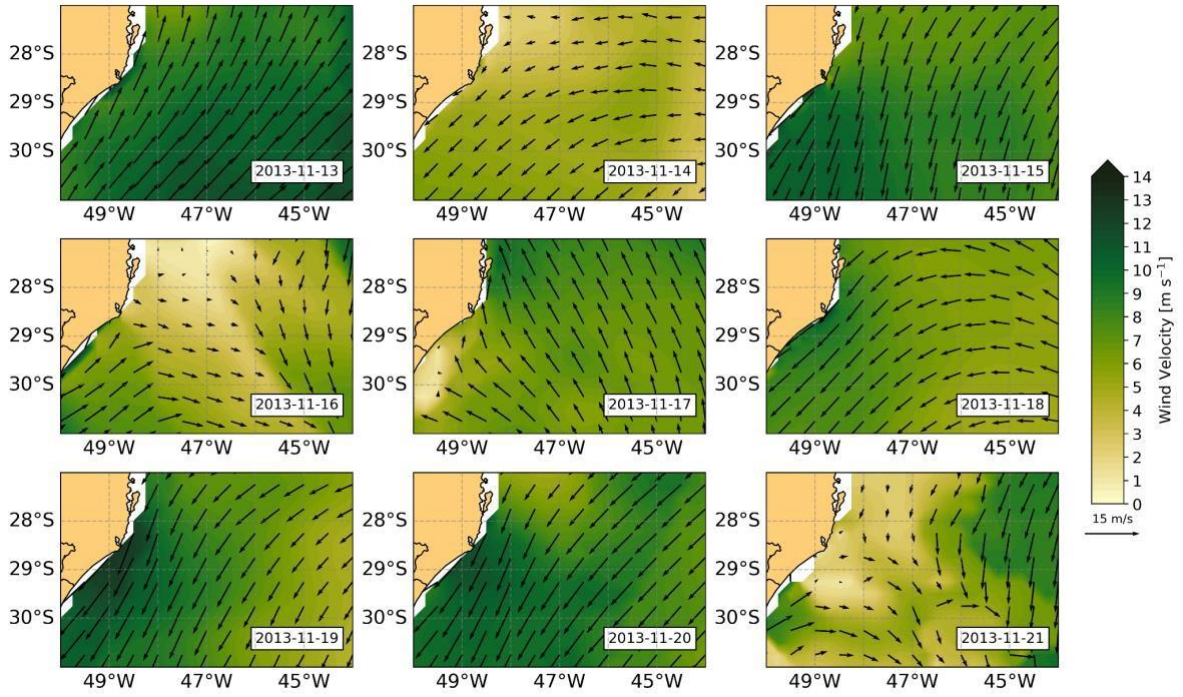

Figure 6: Daily sea surface winds velocity magnitude (colors) and vectors for the period between November 13, 2013 and November 21, 2013. The wind data are from the daily NCDC/NOAA Blended Seawinds L4 product.

The meander signature in the salinity data also suggests that once the water is captured by the meander, it remains trapped and the water particles become locked in the BC path (e.g., Matano et al., 2014). Satellite-delivered images also suggest that this fraction of STSW was under the influence of the La Plata River Plume (PRP) as seen in Figure A1 in the Appendix A.

To shed some light on the origins of the low STSW waters reaching the BC region, we show linearly interpolated nutrients (silicate, phosphate, ammonium, nitrate, and nitrite) and chlorophyll-a concentrations near the surface (0-5 m depth) during CERESV cruise in Figure 7. The presented values are in agreement with the values expected for STSW and TW waters presented by Braga et al. (2008), who analyzed the nutrient distribution along the Southwestern South Atlantic continental shelf during austral winter. Comparing the nutrient distributions with the 36 g kg^{-1} isohaline position, the meander signature is clear in the maps of silicate, phosphate, and chlorophyll-a (Figures 7a, b, and f). Note that the shelf waters richer in nutrients are trapped close to the eddy center, while the oligotrophic oceanic waters tend to follow the BC main axis offshore to the 36 g kg^{-1} isohaline. This is especially true for the silicate concentration (Figure 7a), where relatively higher concentrations are found near coastal stations (<150 m), followed by a decrease between the 150 m and 700 m isobaths and an increase near the offshore lobe of the eddy (close to the 36 g kg^{-1} isohaline). According to Braga et al. (2008), silicate is an important tracer of terrestrial inputs (including the PRP), even though it has other sources like upwelling and advection along the shelf break by intermediate waters at higher depths. Therefore, the horizontal pattern observed in Figure 7a seems to reflect the advection of the coastal waters offshore, the entrainment of the plume into the eddy, and the role of the eddy-wind effect on the meander as a mean of accumulating of silicate in its interior.

Another characteristic is that the maximum concentration of nitrate and nitrite are not located in the same regions as the maximum primary productivity associated with the higher concentration of chlorophyll-a (centered at ~700 m isobath). This suggests that shelf waters are trapped long enough to have its nutrients content depleted by organisms' resource consumption due to biological production growth (Woodward and Rees, 2001; Flynn, 2003). To evaluate this possibility, we performed a simple assessment of nitrate consumption inside the meander as a proxy of the time that the coastal waters could be trapped on it. According to Aidar-Aragão et al. (1980), the primary production rate at Cape Santa Marta is near 5 mg C m^{-3} h^{-1}, which is equal to 0.75 mg N m^{-3} h^{-1} using the Redfield ratio. The average nitrate concentration near the meander core is 0.15 µM/L, while a maximum concentration of 0.7 µM/L was found outside the meander, and the climatological reference value on November obtained from the World Ocean Atlas (Garcia et al., 2019) is 1.7 µM/L. Therefore, the required time for nitrate concentrations found outside the meander and the climatological value to reach the values of the meander core due to primary production would be about 46 h and 120 h, respectively. Considering that the primary production is limited by light availability (~12 h day^{-1}), these estimates are close to 4-10 days, which is in accordance with the meander generation on November 14 as depicted on META3.2exp and the cruise start (November 18). Although these are rough estimates, our results provide evidence of the impact of the cyclones on the biogeochemical water properties.

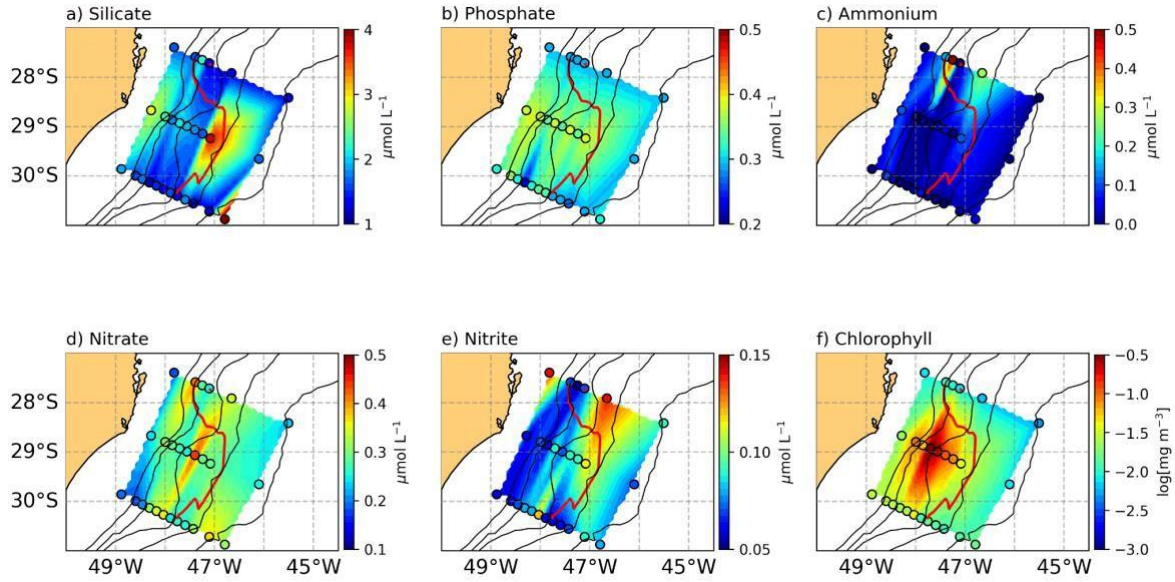

Figure 7: Average near-surface (0-5 m) linearly interpolated distribution of the concentration of (a) silicate, (b) phosphate, (c) ammonium, (d) nitrate, (e) nitrite and (f) chlorophyll-a. The thick red line indicates the salinity of 36 g kg^{-1} at 5 m depth. The black circles indicate where CTD profiles and water samples were taken. Black contours indicate the isobaths of 150, 200, 700, 2000 and 3000 meters.

4. The Brazil Current Variability and Cyclone Recurrence

In the previous section, we showed the BC cyclonic meanders' water mass patterns, physical dimensions, and their role in the shelf-slope mass exchanges. However, two important questions regarding their temporal variability remain open: (1) How often do the cyclonic eddies occur at the vicinities of Cape Santa Marta? (2) How much do these features account for the BC variability in the study region?

4.1. Cyclone formation and properties from SSH

To answer the first question, we show the 0.25° binned histogram of cyclone's formation (i.e, their first detection point) from META3.2exp in Figure 8a. This result shows two distinct peaks of cyclone generation near the Cape Santa Marta, one centralized near 28.5°S-47.5°W and the other site at 30.5°S-48.5°W. We categorized as eddy events all the eddies generated inside a circle with 1° radius (~ 110 km) encompassing the two peaks of the cyclone formation. We identified a total of 342 eddies between 1993 and 2021, 140 (~5 year^{-1}) of which were formed between 28.5°S-47.5°W (hereinafter SM*n*) and 202 (~7 year^{-1}) were formed near 30.5°S-48.5°W (hereinafter SM*s*).

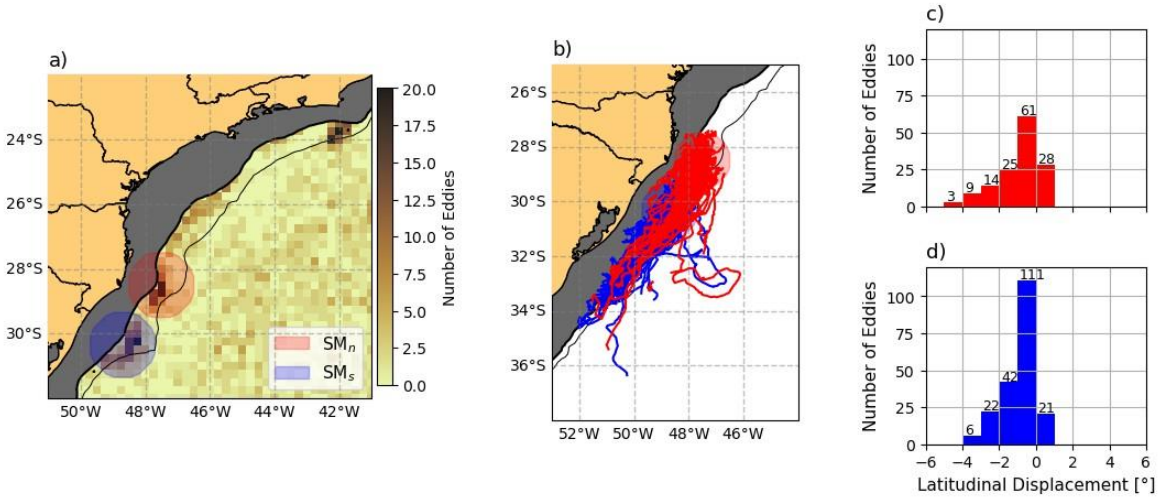

Figure 8: (a) Binned (0.25° x 0.25°) 2D histogram map for cyclones formations (first detection point) from META3.2exp on the South Brazil Bight highlighting two peaks near Cape Santa Marta; b) Pathways from the SM*n* (red) and SM*s* (blue); Distribution of the latitudinal displacement of the SM*n* (c) and SM*s* (d). The gray mask covers areas shallower than 150 m (a,b), and the thin black contour denotes the 200 m isobath.

The eddies propagation seems to be closely related to the BC path following the continental slope and the external portion of the shelf (Figure 8b). The majority of the events on both sites (61% for SM*n* and 75% for SM*s*) remained within 2° of southward displacement from their site origin (Figures 8c and 8d). Nearly 18% of the SM*n* events have a southward displacement above 2 latitudinal degrees from their origin, in comparison to 13% of the SM*s*. Furthermore, 20% (10%) of the SM*n* (SM*s*) propagate northward, with a maximum displacement of one latitudinal degree.

On average, both SM*n* and SM*s* events last for 37 days (Figure 9) before they lose their surface signature. Apparently, these eddies do not detach from the BC and remain as meanders, hence they follow the BC main axis during their lifetime (Figure 8b). The average lifetime of these eddies is smaller in comparison to general eddies on SBB, where according to Rocha and Simoes-Sousa (2022) the lifetime of cyclones is nearly 47 days. Surface characteristics of the eddies generated at both sites seem to be very similar, SM*s* are slightly larger (mean radius of 56.5 ± 19.8 km) than the SM*n* (mean radius of 53.6 ± 16 km) and with a slightly higher SLA amplitude (5 cm for SM*s* in comparison to 3 cm of SM*n*). However, despite their amplitude, the differences in eddies properties on each site are not statistically significant for a 95% confidence interval (p-value > 0.05).

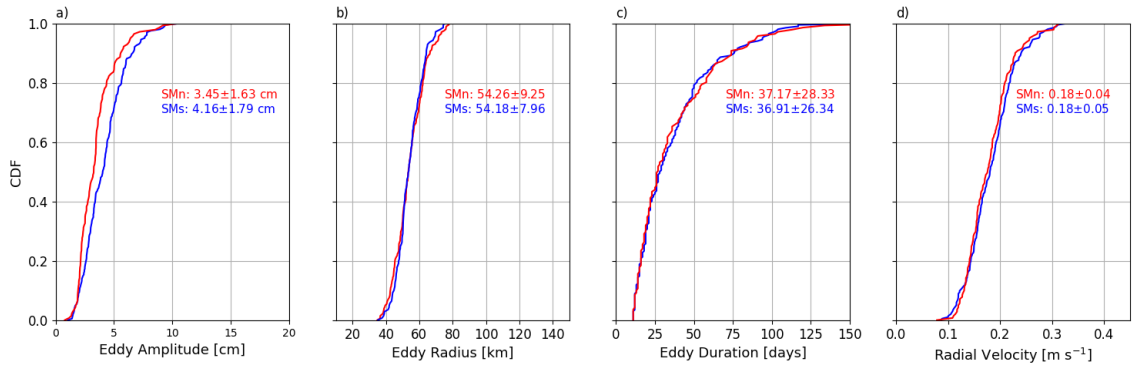

Figure 9: Cumulative density functions (CDF) for eddy amplitude (a), radius (b), lifetime (c), and radial velocity (d). Red lines are for SM*n* events and blue lines are for SM*s* events. The average value and the standard deviation are plotted in each subpanel.

The eddy generation occurs throughout the year in both areas, but seasonal variations are observed in their generation ratio (Figure 10). The maximum ratio of eddies generation occurred between July and September (austral winter to spring), and the minimum ratio is found in February (austral summer). In the modeling study of Combes et al. (2023), the authors investigated slope eddies generated near Cape Santa Marta and also found a minimum number of eddies coverage in February and a maximum in August. Napolitano et al. (2021) and Uchoa et al. (2023) observed higher formation rates of the Vitória Eddy (~21°S) when the BC is at its weakest volume transport. We highlight that the BC volume transport between 24°S-35°S is lowest during winter months (Schmid and Majumder, 2018), and this may be connected to the different number of eddies of Figure 10, requiring further investigations.

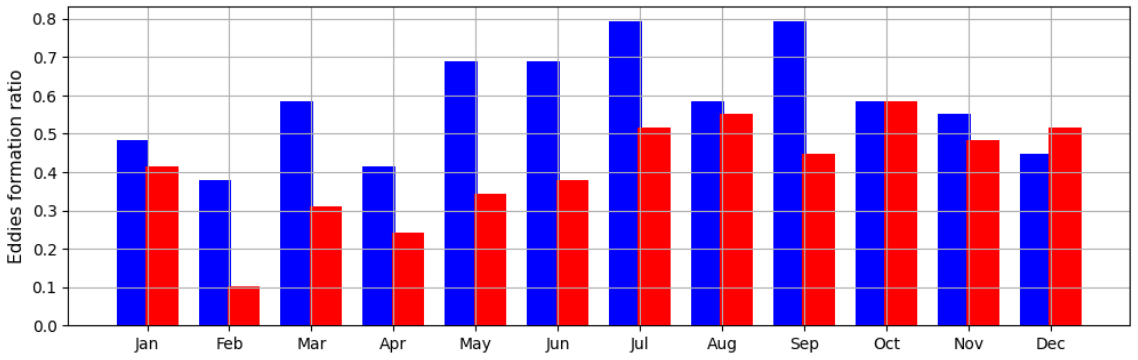

Figure 10: Seasonal cycle of the formation ratio for SM*n* (red) and SM*s* (blue).

Mechanisms such as topographic interactions, barotropic and baroclinic instabilities are able to promote the growth of mesoscale eddies and may contribute to enlarging the Santa Marta Eddies. The influence of topography in destabilizing the BC has been well reported near Cape Frio (23°S) and Cape São Tomé (22°S). Silveira et al. (2008) and Rocha et al. (2014) studied the dynamics of the eddies generated on these two capes and found that the main mechanism that contributes to their growth is baroclinic instability. Brum et al. (2017) studied the energetics of BC near the Rio Grande Cone region (30°S-35°S) and found that baroclinic instability is the main source of eddy kinetic energy in this area. Mano et al. (2009) used numerical modeling to show that barotropic instability also becomes relevant when growth begins near Cape Frio. Barotropic instabilities are known to increase in regions where

the gradient of the absolute vorticity from large-scale currents almost vanishes (Aguedjou et al., 2019; Dossa et al., 2022). Following the ideas of Dossa et al. (2022), we estimate the seasonal cycle of the absolute vorticity gradient (*C*) from altimetry superposed with the formation position of each eddy detected and assess the variation of the number of eddies formed in each region as a function of the absolute vorticity gradient (Figure 11).

The spatial distribution on the seasonal maps does not show a pronounced cycle. We observe a dipole pattern near 29°S-47.5°W, close to SM*n* formation. This pattern is present in all seasons, and the majority of SM*n* are formed near the transition zones between the two cores, and some over negative values. Low vorticity gradients dominate the region of SM*s*, and most of the eddies are generated in areas where C is close to 0. We computed the vorticity gradient at the position of each detected eddy (Figure 11e). The proportion of SMs eddies generated in areas of weak C values (-.3 to .3 x 10^{-10} m^{-1} s^{-1}) is ~65%. This indicates that barotropic instability, due to the horizontal shear of the surface currents, might be more important at SM*s* than at SM*n*, where only 20% of eddies are associated with weak C values, and there is a tendency of negative vorticity gradients on the formation points (~50%). Additionally, unlike the generation of eddies, the vorticity gradient does not exhibit a seasonal cycle, suggesting that other mechanisms must be involved in the eddy generation. One possibility is that the BC intensity may play a role in the instability and therefore perhaps is somewhat related to the BC annual cycle. The BC is stronger in the austral summer and weaker in the austral winter (Schmid and Majumder, 2018).

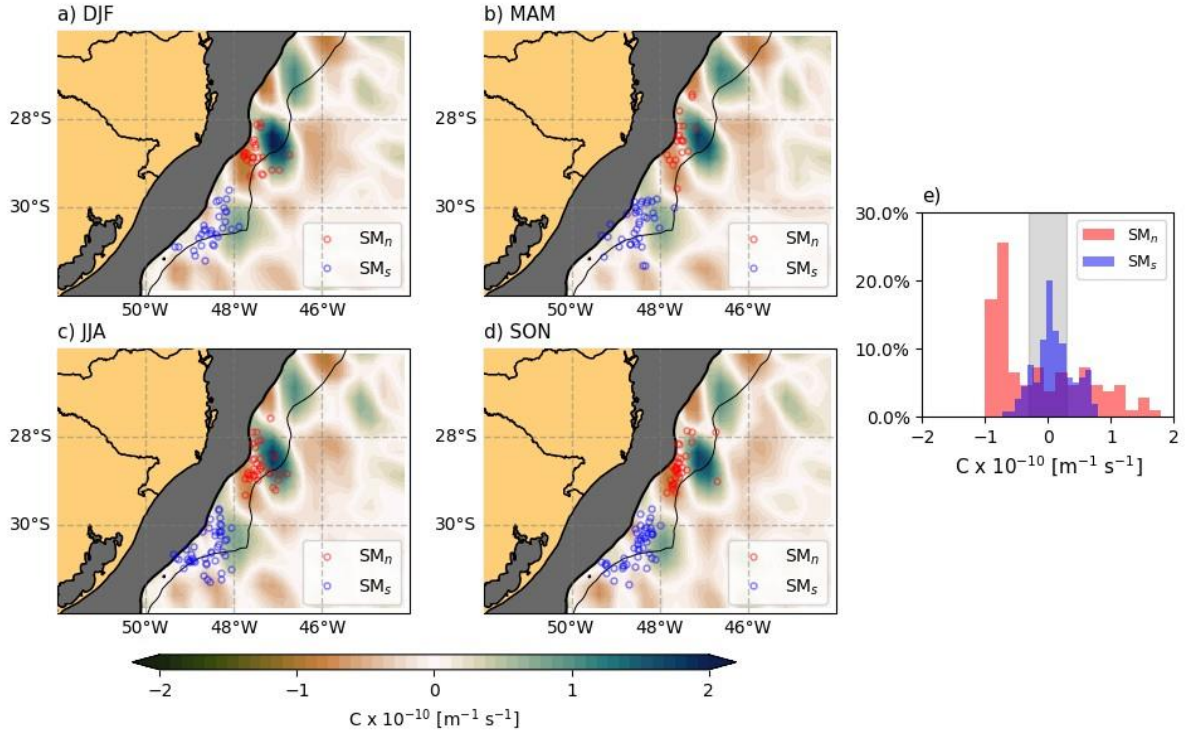

Figure 11: (a-d) Seasonal maps of the gradient of absolute vorticity from large-scale currents from altimetry superimposed with SM*n* (red) and SM*s* (blue) generation points; e) Percentage of the number of detected eddies as a function of the gradient of large-scale vorticity at eddy generation points. The gray shaded area on (e) indicates *C* values between -.3 and .3 × 10^{-10} m^{-1} s^{-1}. The gray mask on (a-d) covers areas shallower than 150 m and the thin black contour is the 200 m isobath.

From the estimates of the eddies growth rate (Figure 12), we observe that both SM*s* and SM*n* present an initial growth rate of ~0.1 day^{-1} and during the first five days, they grow approximately 0.05 day^{-1}. During this initial stage, the eddies also have similar phase speeds (0.09 - 0.1 m s^{-1}). These values are very similar to the growth rate and phase speeds of Cape Frio Eddies (CFE) and Cape São Tomé Eddies (CSTE) obtained in the works of Silveira et al. (2023) and Uchoa et al. (2023). According to Silveira et al. (2023) CFE and CSTE have a quasi-stationary growth and studies have shown that they can migrate northward, southward, and pair with anticyclonic rings giving rise to a dipole structure (Mill et al., 2015; Guerra et al., 2018; Uchoa et al., 2023).

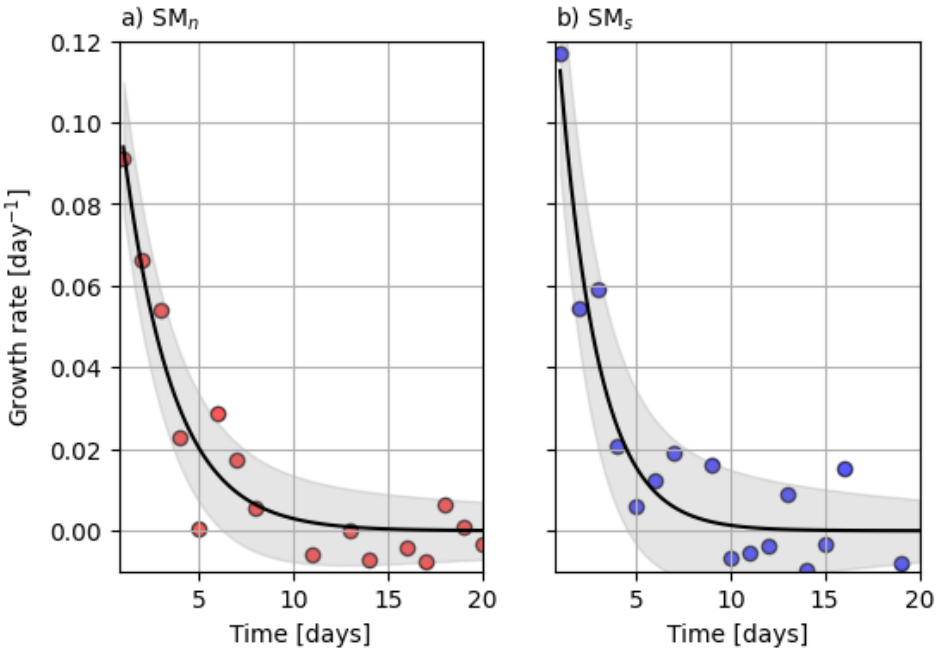

Figure 12: Growth rates of the SM*n* (a) and SM*s* (b) eddies. The solid black curves represent the exponential adjusted rate based on the eddy radius. The shaded envelopes represent the error of the adjusted curve. The colored circles are the mean value based on the analyzed eddies.

In Figure 13 we highlight two different scenarios in which the propagation of the Cape Santa Marta eddies can occur differently: (I) when there is no interaction between the cyclones with anticyclonic structures, so they grow with a very small propagation (Figures 13a-c); (II) when there is a formation of a dipole structure between the cyclones with anticyclonic eddies, which may lead to a southward advection of both features within the BC (Figures 13d-f). During their initial 5 days, the eddies had very similar growth rates of 0.11 day^{-1} (case I) and 0.13 day^{-1} (case II), with average phase speeds of 0.06 m s^{-1} and 0.1 m s^{-1}, respectively. However, in case I the SM*n* latitudinal displacement in the period of ~40 days is 0.2 degrees, while in case II this value is closer to 2.5 latitudinal degrees.

The interaction of BC cyclonic eddies with anticyclones resulting in dipoles has been well reported previously in the northern domain of SBB (Guerra et al., 2018; de Paula et al., 2021; Silveira et al., 2022). These studies mention a dipole structure formed due to the pairing of Cape Frio eddies with anticyclonic rings that may come from Agulhas retroflection and reach the northern portion of SBB. From Figures 13d-13f we also note that dipole structures can be formed on the southern portion of SBB due to the pairing of an SM*n* meander and an anticyclone. A tendency of southwestward propagation results from this

association, as previously said. In the EAC, eddies dipole have been described as a mechanism by which coastal and offshore chlorophyll are linked (Ismail and Ribbe., 2019; Malan et al., 2023), due to the generation of cross-shelf jets that advects coastal waters further offshore. Using the same dipole example of Figures 13d-13f, on Figure A2 (Appendix A), we show a snapshot from MODIS-Aqua in which a flament with higher chlorophyll concentration than the surrounding waters is associated with the jet generated from to the pairing of the eddies. This suggests that the straining of BC mesoscale activity near the Cape Santa Marta might give rise to fine-scale structures, such as enriched Chl-a filaments, which can export shelf waters further offshore. A similar pattern associated with the BC has been reported to the south, near the Brazil- Malvinas Confluence region (~38°S), where filaments of 70 km wide and 20 m deep were measured *in situ* (Manta et al., 2022).

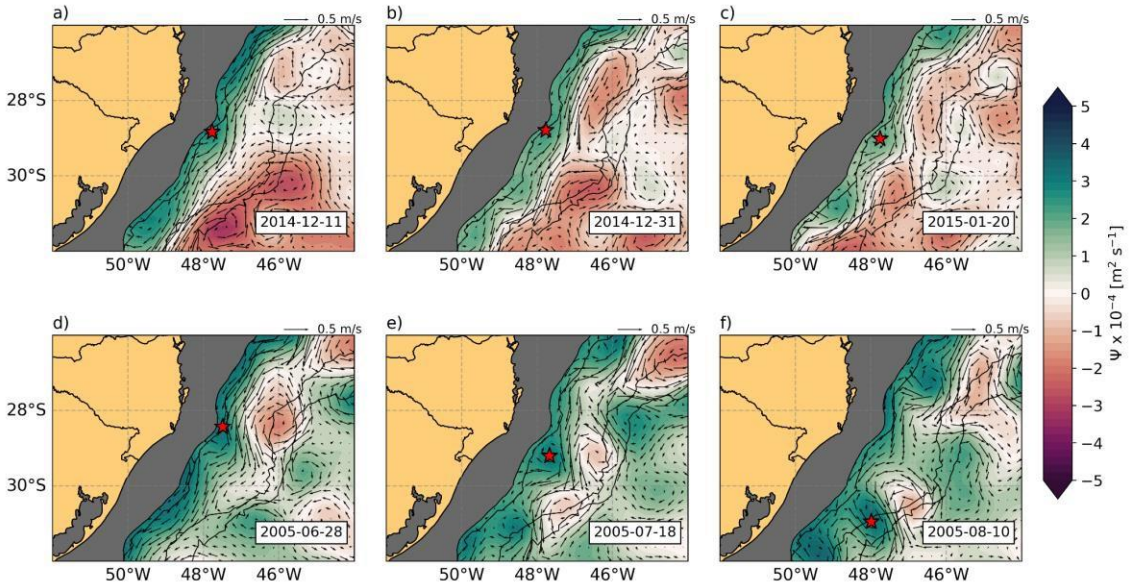

Figure 13: Altimeter derived stream function (ψ) and velocity vectors during examples of meandering growing and propagation cases observed for the Santa Marta Eddies. (a-c) presents a quasi-stationary case and (d-e) presents a dipole-structure propagation. Red stars are the eddies' center position from META3.2exp. The gray mask covers areas shallower than 150 m and the thin black contours are the 200 m, 2500 m and 3000 m isobaths.

4.2. Brazil Current variability from moored instruments

In this section, we use the WOCE mooring lines array (Figure 1) to investigate how much these eddies account for the BC variability in our study area. These current meters' time series were extensively explored in the literature and had their velocity signal already discussed (e.g., Müller et al., 1998; Hogg et al., 1999; Rocha et al., 2014). In that sense, we computed the Empirical Orthogonal Functions (EOF) of the time series velocity array to characterize the subinertial variability. The cross-sectional velocity component was obtained by rotating the velocity vectors approximately 30° clockwise, which represents the velocity parallel to 200 m and 1000 m isobaths. Moreover, this was computed only for the common period to all mooring records (May 1, 1991 to November 24, 1992). The obtained time series of the observed and mode-fitted cross-sectional velocity components are displayed as Hovmoller's diagrams in Figure 14. BW333 mooring is located near the core of the BC (Figure 14a) and hence presents an intense along-shore southward velocity in the upper 900 m in comparison with the other moorings. The flow pattern observed at BM334 (Figure 14d) is quite similar to the one at BW333, with lower velocity values, also suggesting the influence of the BC at this

mooring. For the moorings BE335 (Figure 14g) and W906 (Figure 14j), some flow inversions occur in the upper 1000 m and northward along-shore velocities are observed. The mode-fitted extrapolated velocities presented a good agreement with the observed field, and the average root mean squared error (RMSE) between the fields was less than 0.05 m s^{-1}, with an exception for the BW333 mooring, where this value was 0.06 m s^{-1}, which may be due to the BC higher variability at this mooring. Therefore, we opted to use the extrapolated field to compute the EOFs.

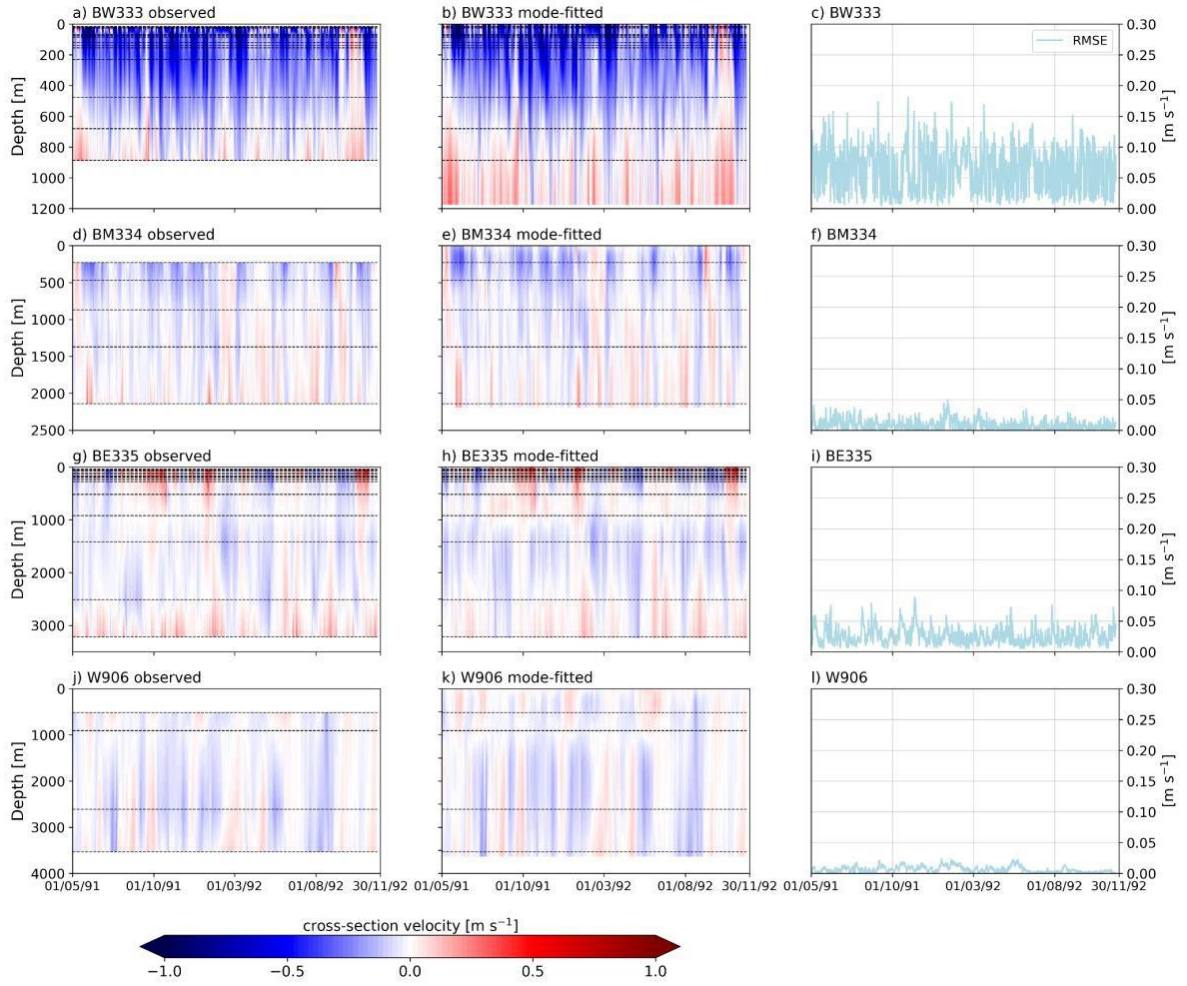

Figure 14: Cross-sectional velocity in each mooring for the period of May 1, 1991 - November 24, 1992. Observed feld (left column) with the mean instrument's depths (horizontal dashed lines) and six mode-fitted velocity (center column) in each deployment. The vertical RMSE of the mode-fitted signal at the instrument's depths is displayed in the right column.

The mean cross-sectional velocity field (Figure 15a) shows part of the BC signal in the upper 1000 m over the onshore portion of the continental slope. Also, the positive velocity signals at depths greater than 2500 m may be related to the BC re-circulation cell and the Antarctic Bottom Water flow (Müller et al., 1998; Hogg et al., 1999). From the EOF results, we observed that more than 80% of the velocity variance was contained in the first 5 modes. However, for the sake of brevity, we will retain our discussion on the first two modes.

The first EOF mode explains 33% of the variance and clearly represents the mesoscale oscillations of the BC (Figure 15b). The spatial structure of this mode resembles a dipole

pattern with the highest values in the BC domain, with a surface intensification, similar to the observed structure of MR03 cruise (Figure 2b). Additionally, the energy spectrum shows that the time series of the first mode is dominated by oscillations with periods of approximately 55 days (Figure 16a). Therefore, the mesoscale oscillations explain at least 1/3 of the variability over the continental slope near the Cape Santa Marta. The second EOF mode explains approximately 14% of the velocity variance (Figure 15c). This mode may be related to the BC recirculation cell (Gordon and Greengrove, 1986), since its structure has a one-direction flow confined in the upper 500 m of water column, followed by two consecutive inversions in the offshore distance, with another core centered at 150 km (on the BE335 mooring at 45.2ºW). Valla et al. (2018) analyzed two synoptic sections at 34.5°S and found a recirculation cell of the BC east of 49°W extending up the 3000 m, with cores centered between 48 and 49°W and 46.5 and 45°W. These authors also suggested that this recirculation cell extends as far north as 27°S, so the second EOF signal associated with periods ~70 days (Figure 16b) may be associated to this pattern.

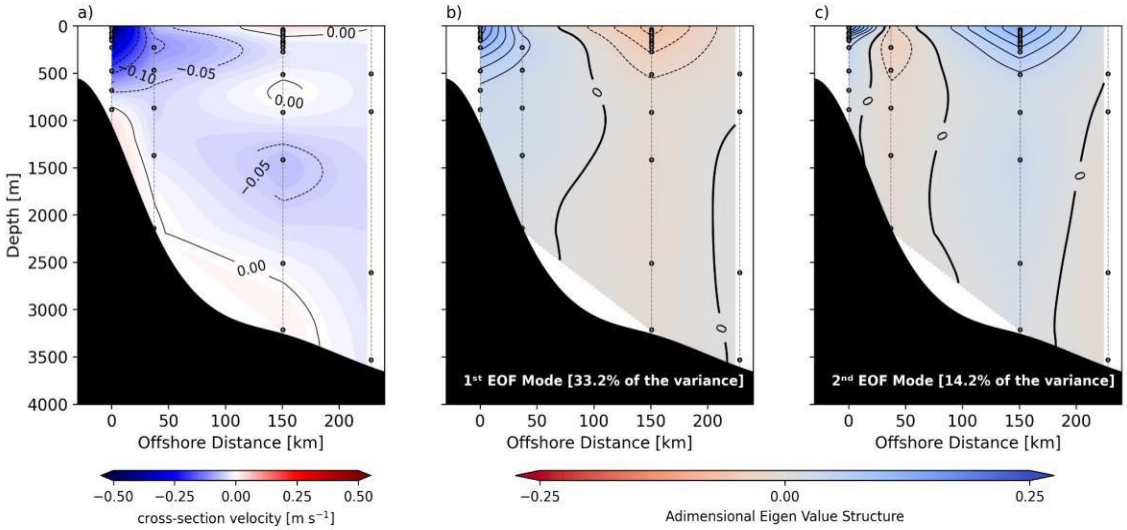

Figure 15: Average mean cross-sectional velocity array (a); the first (b) and second (c) statistical mode eigen structures. The gray dashed lines represent the mooring lines and the circles, the instruments' locations.

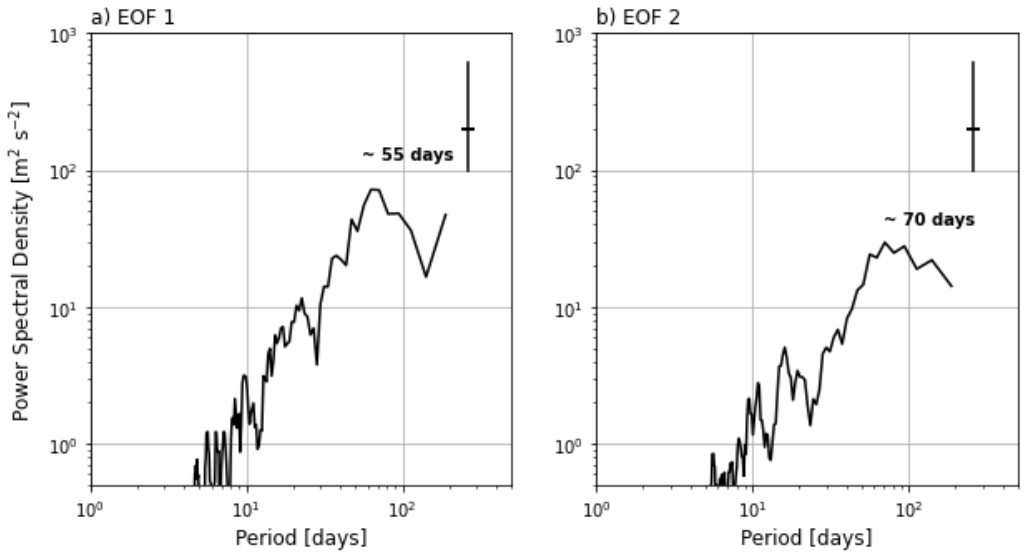

Figure 16: Power Spectral Density obtained for the first (left) and second (right) EOF modal amplitudes from the WOCE mooring array. The vertical bar denotes the 95% confidence interval.

5. Composite Averages of Chlorophyll-a

In section 3 we showed that the presence of cyclonic eddies near CSM could be associated with substantial shelf-slope water exchanges that include nutrient-rich PRP waters, busting the biological production in the BC's oligotrophic waters. Then, in section 4, we verified that eddies near CSM are a recurrent phenomenon that can happen 5-7 times per year. Therefore, a question that remains open is whether these hundreds of eddies also contribute to the sustainment of high biological productivity.

In order to address this question, we now analyze composite averages of chlorophyll- a spatial anomalies in eddy-centric coordinates. Due to GlobColour data availability, we selected only the eddies generated after January 1997. This procedure resulted in a total of 105 (156) eddies and 583 (831) valid images for the SM*n* (SM*s*).

Figure 17 shows a comparison between the eddy-centric chlorophyll-a snapshot for CERESV eddy (Figures 17a and 17b), and the average composites for SM*n* and SM*s* (Figures17c and 17d). The eddy observed during CERESV cruise presented a clear signal on chlorophyll-a field (Figure 17a), where enriched coastal waters are advected offshore in a cyclonic sense. This lateral stirring of chlorophyll-a due to the eddy rotation is depicted on the anomaly field (Figure 17b). In this plot, a dipole pattern is obtained, with positive values associated with the offshore lobe and negative near the eddy periphery. The average chlorophyll-a anomaly composites for both Santa Marta Eddies sites (Figures 17c,d) shows a SE-NW oriented gradient on Chl-a', perpendicularly to the local coastal orientation and BC axis. These results are qualitatively similar to the dipole pattern characteristic of a response on Chl-a fields due to the eddy advection and lateral stirring. As revealed by Chelton et al. (2011), the azimuthal velocity of the eddies can stir the background Chl-a feld and can imprint an asymmetric Chl-a' dipole. We observe one primary core occupying most of the eddy core area, and a secondary core in the periphery of the eddy, just as observed in Figure 17b for the CERESV cyclone.

Note that the asymmetric dipole pattern is visualized in all seasons, except during austral autumn (Figure 18). The reasons for the lack of autumn dipoles remain unknown. However, we speculate that the relatively smaller number of eddies generated in March and April could have a controlling effect. Higher values and gradients of Chl-a' are observed in austral winter (Figure 18c,g), which probably indicates the influence of La Plata River Plume advected northward during southwesterly winds (Piola et al., 2000; Möller Jr et al., 2008; Combes et al., 2021). According to Möller Jr et al. (2008), low salinity waters extend beyond Cape Santa Marta during the austral winter (June-September), and recently Dottori et al. (2023) have reported the influence of these waters on the continental shelf of Santos Basin during austral winter.

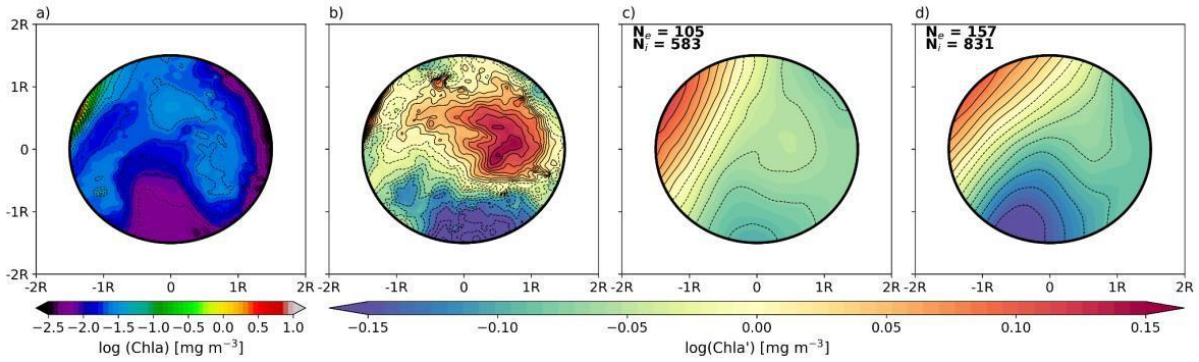

Figure 17: (a) Eddy-centric map of Chl-a for the CERESV cyclone, which trapped STSW on its interior; (b) Eddy-centric map of Chl-a' for the CERESV cyclone; (c) Average composite of Chl-a' for SM*n*; (d) Similar to (c) but for SM*s*. Ne is the number of eddies used to generate the average composite, and Ni is the number of valid satellite images.

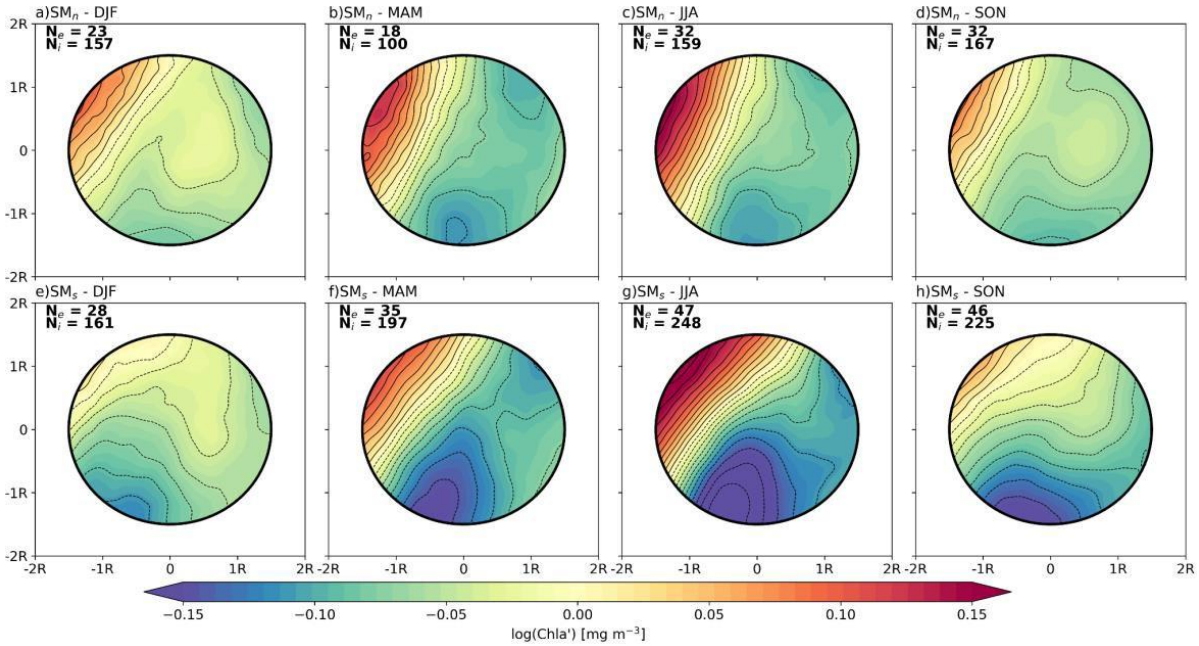

Figure 18: Seasonal averages composites of Chl-a' in eddy-centric coordinates for: (a–d) SM*n*; (e–h) SM*s*. The number of eddies and valid images used for each composite is displayed in each sub-panel. The order is: austral summer, austral autumn, austral winter, and austral spring.

These bio-optical footprints identified indicate that eddy-stirring is an important process that affects the distribution of Chl-a locally and reinforces the results from Section 3.2, showing the ability of the eddies to retain coastal waters in its structure. Also, this is in agreement with the results obtained by the modeling studies of Matano et al. (2014) and Combes et al. (2023), who highlighted the importance of ∼28.5°S and ∼30.5°S as key points for shelf open ocean mass exchange. Our results show that the Santa Marta eddies play a key role in this process and that their influence varies seasonally.

This evidence of lateral advection of shelf waters, obtained through *in situ* data and confirmed by satellite imagery, shows some similarities between the SM eddies and frontal eddies commonly formed on the shoreward flank of western boundary currents (Suthers et al., 2023). Despite their difference in size (considering that a frontal eddy has a scale of < 50 km

while SM eddies have ~100 km), both structures have a significant role in exporting shelf waters offshore. It is important to point out that those waters may be preconditioned with zooplankton and fish larvae, and their lateral stirring due to the presence of eddies may generate relevant impacts on the local biology. Recently, Calado et al. (2023) analyzed the role of Cape Frio cyclones in the larvae dispersion of sun coral (*Tubastraea* spp.) and found that those larvae trapped inside the eddy traveled almost half the distance in comparison to those that were not trapped. To the best of our knowledge, there are no studies evaluating the impacts of SM eddies on local biology, so we reinforce the importance of studies linking the SM eddies and the biological processes associated near Cape Santa Marta.

6. Summary and Conclusions

In this paper, we described the general characteristics of the BC cyclonic meandering near Cape Santa Marta (27°S-31°S). A wide range of *in situ* observations was used to provide an overview of the meanders' water masses circulation, surface temperature, salinity, and nutrients. In addition, the Santa Marta eddies formation sites, variability, and their impact on primary production were also addressed from satellite data.

The top-bottom quasi-synoptic velocity measurements depicted cyclonic meanders over the continental slope with diameters larger than 100 km. Moreover, the eddies presented velocity signals extending to approximately 1500 m depth, which highlights the dynamical coupling of the upper 500 m flow with the intermediate one (500-1500 m). The observed BC eddies seem to trap and recirculate a small portion (~1.5 to 2 Sv) of the BC main flow, which consists of TW, SACW, AAIW, and UCDW. Additionally, we presented observational evidence of the influence of the cyclonic meanders in the shelf- open ocean exchanges. The salinity horizontal distributions combined with the nutrient concentrations led us to conclude that the BC meanders actively influence the STSW transport to the open ocean, enhancing the primary productivity at the photic zone over the continental slope.

From satellite imagery, the cyclonic meandering of the BC at Cape Santa Marta is associated with two distinct regions of cyclone formations, one at 28°S and the other at 30°S, where on average, 5 and 7 eddies are generated per year in each site, respectively. In addition, these eddies have a shorter lifetime (~37 days) in comparison with the BC eddies from Cape Frio and Cape Santa Marta (~47 days). An EOF analysis computed from an array of mooring lines equipped with current meters shows that the BC mesoscale activity explains approximately 1/3 of the variance on the continental slope.

Furthermore, a set of chlorophyll-a images suggests that the lateral stirring of enriched coastal waters in these eddies is a recurrent phenomenon, providing evidence that the BC mesoscale eddies could have a significant impact on the shelf-deep ocean water exchanges along the entire Southern Brazilian coast (e.g., Figure A1). This entrainment may also contain enriched waters from the La Plata River plume, which modulate marine ecosystems and influence fisheries stocks, revealing the economic importance of these meanders and the need to understand those features.

Our study was just the beginning of the challenging task that is describing the mesoscale cyclonic eddies generated by the BC near CSM and there are still many issues that have not been explored in the present study. Nevertheless, we believe this study could be a starting point for future studies regarding these eddies' genesis and formation. Also, due to the limitation of the observational dataset, we could not quantitatively address some essential points related to

the observed cross-shelf exchanges and their biological impacts. Therefore, we point out that future observational programs and modeling efforts should seek to quantify the relative importance of the wind forcing and smaller-scale processes compared to the mesoscale variability, and address quantitatively the biological and chemical effects of these eddies on the region.

7. Data Availability Statement

The datasets from CERESV and MR03 used in this study are available upon request to the corresponding author.

8. Acknowledgments

We would like to thank PETROBRAS for their partnership and permission to use and display proprietary data of the CERES cruise. J. P. M. A. acknowledges the financial support from CAPES (Process number 88887.921525/2023-00). I.C.A.S. and P.S.B. acknowledge support from CNPq (Project HIDROSAN I, 405593/2021-0) and FAPESP (Project HIDROSAN II, 2021/13124-6). T. C. B. gratefully acknowledges the funding from the NOAA's Global Ocean Monitoring and Observing program (FundRef number 100007298); NOAA's Climate Program Office, Climate Observations and Monitoring, and Climate Variability and Predictability programs under NOFO NOAA-OAR-CPO- 2021-2006389 with additional NOAA Atlantic Oceanographic and Meteorological Laboratory support. This research was carried out in part under the auspices of the Cooperative Institute for Marine and Atmospheric Studies, a cooperative institute of the University of Miami, and the National Oceanic and Atmospheric Administration (NOAA), cooperative agreement NA 20OAR4320472. We thank CMES for the distribution of SSALTO/DUACS altimeter and globcolour products, and AVISO for the distribution of META3.2exp.

Appendix A. Origins of the low salinity water and cross-shelf jets

In Figure A1 of this Appendix, we show satellite images that provide evidence that the observed low salinity waters during the CERESV cruise were under the influence of the PRP or a mixing between PRP waters and Brazilian shelf waters. Figure A1a shows the weekly salinity composite with 0.25° horizontal resolution during the CERESV survey obtained from the Soil Moisture and Ocean Salinity mission (SMOS, Kerr et al. 2010). This figure shows a low salinity tongue extending northward from the Plata River mouth, and waters with salinity less than 33.5 g kg^{-1} (red line on Figure A1a), which delimits the plume according to Piola et al. (2005), reaching latitudes as far as 30°S. Also, there is an accordance between the 35 g kg^{-1} isohaline observed during the cruise (dashed black line) and the SMOS data (continuous black line). Sea Surface Temperature (SST) from the Multi-scale Ultra-high Resolution (MUR, Chin et al. 2017) product at 0.01° horizontal resolution also shows low-temperature waters extending from Plata River mouth till Cape Santa Marta near the coast (Figure A1b). Furthermore, chlorophyll estimates from Globcolour show enriched chlorophyll waters extending near the coast from the Plata River mouth to the Cape Santa Marta (Figure A1c).

Figure A2 depicts a snapshot of chlorophyll concentration from MODIS Acqua (horizontal resolution of 4 km) for the same dipole of Figures 13d-13f on August 5, 2005. The chlorophyll map overlaid with geostrophic velocity vectors (Figure A2a) shows a patch of higher chlorophyll concentrations associated with the jet generated from the fused eddies lobes in the dipole. In this snapshot, it is possible to note the extrusion of coastal waters as a filament associated with the dipole structure. Additionally, there is a partial encircle of the anticyclone with higher chlorophyll waters in comparison to the surrounding areas. Cross-shelf geostrophic velocities obtained from an along-shelf line show maximum velocities of $\sim$0.4 m s^{-1} and an increase of chlorophyll concentration near the jet core (Figure A2b).

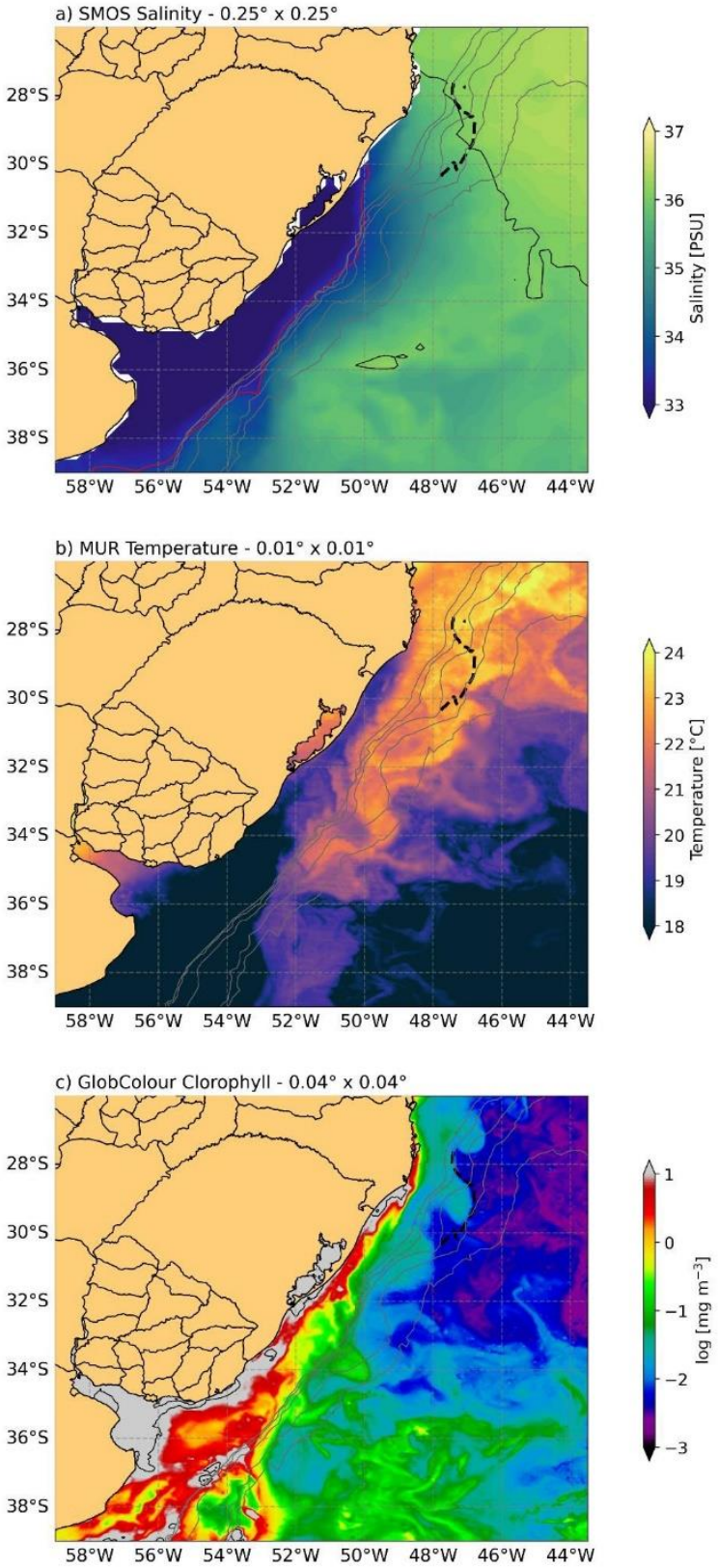

Figure A1: Satellite images obtained for surface salinity (a); SST (b) and chlorophyll-a (c) during the CERESV survey. Red and black lines on (a) delimits the isohalines of 33.5 g kg^{-1} and 36 g kg^{-1}, respectively. Dashed black lines in all the panels represent the observed 36 g kg^{-1} isohaline at 5 m. The thin gray contours are the 150 m, 200 m, 700 m, 2000 m and 3000 m isobaths.

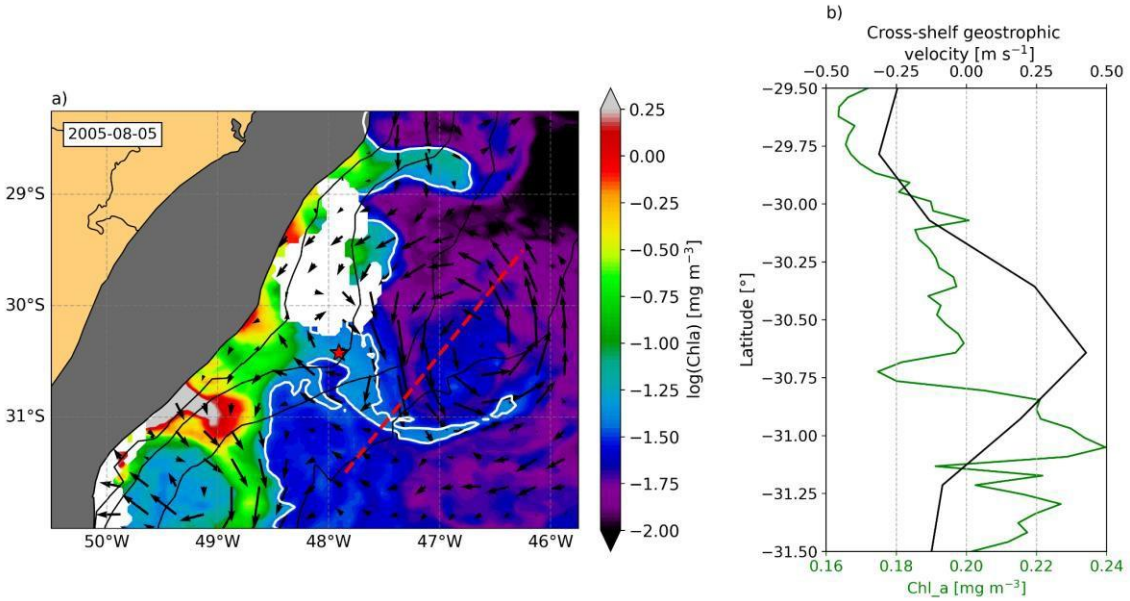

Figure A2: (a) Chlorophyll (MODIS-Acqua) and geostrophic velocity vectors (altimetry) snapshot on August 5, 2005. White areas denote missing data, the red star is the SM*n* position from META3.2exp, the thick white line is the 0.23 mg m^{-3} chlorophyll contour, the black contours are the 200 m, 700 m and 3000 m isobaths, and the gray mask covers areas shallower than 150 m. (b) Cross-shelf geostrophic velocities and chlorophyll concentration observed along the dashed red line on (a).

References

Aguedjou, H., Dadou, I., Chaigneau, A., Morel, Y., Alory, G., 2019. Eddies in the Tropical Atlantic Ocean and their seasonal variability. Geophysical Research Letters 46, 12156–12164.

Aidar-Aragão, E., Teixeira, C., Vieira, A., 1980. Produção primária e concentração de clorofila-a na costa brasileira (Lat. 22º 31'S-Long. 41º52'W a Lat. 28º43'S-Long. 47º57'W). Boletim do Instituto Oceanográfico 29, 09–14.

Amorim, J.P., da Silveira, I.C., Borges-Silva, M., Souza-Neto, P.W., Belo, W.C., Lazaneo, C.Z., Bernardo, P.S., Dottori, M., Martins, R.P., Moreira, D.L., 2023. A vertical-mode extrapolation scheme applied to the Brazil Current domain: quasi-synoptic scenarios. Ocean and Coastal Research 70.

Arruda, W.Z., da Silveira, I.C., 2019. Dipole-induced central water extrusions south of Abrolhos Bank (Brazil, 20.5°S). Continental Shelf Research 188, 103976.

Beckers, J.M., Rixen, M., 2003. EOF calculations and data filling from incomplete oceanographic datasets. Journal of Atmospheric and Oceanic technology 20, 1839–1856.

Biló, T.C., da Silveira, I.C.A., Belo, W.C., de Castro, B.M., Piola, A.R., 2014. Methods for estimating the velocities of the Brazil Current in the pre-salt reservoir area off southeast Brazil (23 S–26 S). Ocean Dynamics 64, 1431–1446.

Boebel, O., Davis, R., Ollitrault, M., Peterson, R., Richardson, P., Schmid, C., Zenk, W., 1999. The intermediate depth circulation of the western South Atlantic. Geophysical Research Letters 26, 3329–3332.

Boyer, T., Garcia, H., Locarnini, R., Zweng, M., Mishonov, A., Reagan, J., Weathers, K., Baranova, O., Seidov, D., Smolyar, I., 2018. World Ocean Atlas 2018 .

Braga, E.S., Chiozzini, V.C., Berbel, G.B., Maluf, J.C., Aguiar, V.M., Charo, M., Molina, D., Romero, S.I., Eichler, B.B., 2008. Nutrient distributions over the Southwestern South Atlantic continental shelf from Mar del Plata (Argentina) to Itajaí (Brazil): Winter– summer aspects. Continental Shelf Research 28, 1649–1661.

Brum, A.L., de Azevedo, J.L.L., de Oliveira, L.R., Calil, P.H.R., 2017. Energetics of the Brazil current in the Rio Grande Cone region. Deep Sea Research Part I: Oceanographic Research Papers 128, 67–81.

Calado, L., Gangopadhyay, A., Silveira, I.d., 2008. Feature–oriented regional modeling and simulations (FORMS) for the western South Atlantic: Southeastern Brazil region. Ocean Modelling 25, 48–64.

Calado, L., Silveira, I.C.A.d., Gangopadhyay, A., Castro, B.M., 2010. Eddy–induced upwelling off Cape São Tomé (22°S, Brazil). Continental Shelf Research 30, 1181–1188.

Callbeck, C.M., Lavik, G., Stramma, L., Kuypers, M.M., Bristow, L.A., 2017. Enhanced nitrogen loss by eddy-induced vertical transport in the off shore Peruvian oxygen minimum zone. PLoS One 12, e0170059.

Campos, E.J., Goncalves, J., Ikeda, Y., 1995. Water mass characteristics and geostrophic circulation in the South Brazil Bight: Summer of 1991. Journal of Geophysical Research: Oceans 100, 18537–18550.

Campos, E.J.D., Velhote, D., Silveira, I.C.A.d., 2000. Shelf break upwelling driven by Brazil Current cyclonic meanders. Geophysical Research Letters 27, 751–754.

Campos, P.C., Möller Jr, O., Piola, A., Palma, E., 2013. Seasonal variability and coastal upwelling near Cape Santa Marta (Brazil). Journal of Geophysical Research: Oceans 118, 1420–1433.

Calado, L., Cosenza, B., Moraes, F., Mizrahi, D., Xavier, F. C., Batista, D., Calazans, S., Araújo, F., Coutinho, R. 2023. Modeling the larvae dispersion of sun coral in the Brazil current off Cape Frio: A cyclonic eddy scenario. Plos one, *18*(12), e0295534.

Castelao, R.M., Campos, E.J., Miller, J.L., 2004. A modelling study of coastal upwelling driven by wind and meanders of the Brazil Current. Journal of Coastal Research 20, 662– 671.

Castro, B., Miranda, L., 1998. Physical oceanography of the western Atlantic continental shelf located between 4 N and 34 S. The sea 11, 209–251.

Chelton, D.B., Gaube, P., Schlax, M.G., Early, J.J., Samelson, R.M., 2011. The influence of nonlinear mesoscale eddies on near-surface oceanic chlorophyll. Science 334, 328– 332.

Chin, T.M., Vazquez-Cuervo, J., Armstrong, E.M., 2017. A multi-scale high resolution analysis of global sea surface temperature. Remote sensing of environment 200, 154–169.

Combes, V., Matano, R.P., Palma, E.D., 2021. Circulation and Cross Shelf Exchanges in the Northern Shelf Region of the Southwestern Atlantic: Kinematics. Journal of Geophysical Research: Oceans 126, e2020JC016959.

Combes, V., Matano, R.P., Palma, E.D., 2023. Circulation and Cross-Shelf Exchanges in the Northern Shelf of the Southwestern Atlantic: Dynamics. Journal of Geophysical Research: Oceans n/a, e2023JC019887. URL: https://agupubs.onlinelibrary.wiley.com/doi/abs/10.1029/2023JC019887,doi:https://doi.org/10.1029/2023JC019887.

Dossa, A.N., Costa Da Silva, A., Hernandez, F., Aguedjou, H., Chaigneau, A., Araujo, M., Bertrand, A., 2022. Mesoscale eddies in the southwestern tropical Atlantic. Frontiers in Marine Science 9.

Dottori, M., Sasaki, D.K., Silva, D.A., Del-Giovannino, S.R., Pinto, A.P., Gnamah, M., Santos, A.D., da Silveira, I.C., Belo, W.C., Martins, R.P., et al., 2023. Hydrographic structure of the continental shelf in Santos Basin and its causes: The SANAGU and SANSED campaigns (2019). Ocean and Coastal Research 71.

Everett, J. D., Macdonald, H., Baird, M. E., Humphries, J., Roughan, M., & Suthers, I. M. (2015). Cyclonic entrainment of preconditioned shelf waters into a frontal eddy. Journal of Geophysical Research: Oceans, *120*(2), 677-691.

Fischer, J., Visbeck, M., 1993. Deep velocity profiling with self-contained ADCPs. Journal of atmospheric and oceanic technology 10, 764–773.

Flierl, G., McGillicuddy, D.J., 2002. Mesoscale and submesoscale physical biological interactions. The sea 12, 113–185.

Flynn, K.J., 2003. Modelling multi-nutrient interactions in phytoplankton; balancing simplicity and realism. Progress in Oceanography 56, 249–279.

Garcia, H., Weathers, K., Paver, C., Smolyar, I., Boyer, T., Locarnini, M., Zweng, M., Mishonov, A., Baranova, O., Seidov, D., et al., 2019. World Ocean Atlas 2018. Vol. 4: Dissolved inorganic nutrients (phosphate, nitrate and nitrate+ nitrite, silicate) .

Garfield, N.I., 1990. The Brazil Current at subtropical latitudes. Ph.D. thesis. University of Rhode Island. Rhode Island.

Gordon, A.L., Greengrove, C.L., 1986. Geostrophic circulation of the Brazil Falkland confluence. Deep Sea Research Part A. Oceanographic Research Papers 33, 573–585.

Grasshoff , K., Kremling, K., Ehrhardt, M., 2009. Methods of seawater analysis. John Wiley & Sons.

Guerra, L.A.A., Paiva, A.M., Chassignet, E.P., 2018. On the translation of Agulhas rings to the western South Atlantic Ocean. Deep Sea Research Part I: Oceanographic Research Papers 139, 104–113.

Hogg, N.G., Siedler, G., Zenk, W., 1999. Circulation and variability at the southern boundary of the Brazil Basin. Journal of Physical Oceanography 29, 145–157.

Ismail, M. F. A., & Ribbe, J. (2019). On the cross-shelf exchange driven by frontal eddies along a western boundary current during austral winter 2007. Estuarine, Coastal and Shelf Science, *227*, 106314.

Jackett, D. R., & McDougall, T. J. (1997). A neutral density variable for the world's oceans. *Journal of Physical Oceanography*, *27*(2), 237-263.

Kerr, Y.H., Waldteufel, P., Wigneron, J.P., Delwart, S., Cabot, F., Boutin, J., Escorihuela, M.J., Font, J., Reul, N., Gruhier, C., et al., 2010. The SMOS mission: New tool for monitoring key elements of the global water cycle. Proceedings of the IEEE 98, 666–687.

Kimura, S., Kasai, A., Nakata, H., Sugimoto, T., Simpson, J. H., & Cheok, J. V. (1997). Biological productivity of meso-scale eddies caused by frontal disturbances in the Kuroshio. ICES Journal of Marine Science, *54*(2), 179-192.

Kimura, S., Nakata, H., & Okazaki, Y. (2000). Biological production in meso-scale eddies caused by frontal disturbances of the Kuroshio Extension. ICES Journal of Marine Science, 57(1), 133-142.

Lavender, S., Antoine, D., Maritorena, S., Morel, A., Barrot, G., Demaria, J., Pinnock, S., 2009. GlobColour—The European service for ocean colour, in: Proceedings of the 2009 IEEE International Geoscience & Remote Sensing Symposium, Cape Town, South Africa, pp. 12–17.

Legeckis, R., Gordon, A.L., 1982. Satellite observations of the Brazil and Falkland currents—1975 1976 and 1978. Deep Sea Research Part A. Oceanographic Research Papers 29, 375–401.

Li, Z., Chao, Y., McWilliams, J.C., 2006. Computation of the streamfunction and velocity potential for limited and irregular domains. Monthly weather review 134, 3384–3394. URL: https://doi.org/10.1175/MWR3249.1.

Luko, C.D., Pereira, F., da Silveira, I.C., Tandon, A., Flierl, G.R., 2022. Eff ects of the seasonality of mesoscale eddies on the planktonic dynamics off eastern Brazil. Dynamics of Atmospheres and Oceans 98, 101299.

Luko, C.D., da Silveira, I., Simoes-Sousa, I.T., Araujo, J.M., Tandon, A., 2021. Revisiting the Atlantic South Equatorial Current. Journal of Geophysical Research: Oceans 126, e2021JC017387.

Malan, N., Roughan, M., Hemming, M., Schaeff er, A., 2023. Mesoscale Circulation Controls Chlorophyll Concentrations in the East Australian Current Separation Zone. Journal of Geophysical Research: Oceans 128, e2022JC019361.

Mano, M.F., Paiva, A.M., Torres Jr, A.R., Coutinho, A.L., 2009. Energy flux to a cyclonic eddy off Cabo Frio, Brazil. Journal of Physical Oceanography 39, 2999–3010.

Manta, G., Speich, S., Barreiro, M., Trinchin, R., de Mello, C., Laxenaire, R., & Piola, A. R. 2022. Shelf Water Export at the Brazil-Malvinas Confluence Evidenced From Combined in situ and Satellite Observations. Frontiers in Marine Science, 9, 857594.

Mason, E., Pascual, A., McWilliams, J.C., 2014. A new sea surface height–based code for oceanic mesoscale eddy tracking. Journal of Atmospheric and Oceanic Technology 31, 1181–1188.

Matano, R., Combes, V., Piola, A.R., Guerrero, R., Palma, E.D., Ted Strub, P., James, C., Fenco, H., Chao, Y., Saraceno, M., 2014. The salinity signature of the cross-shelf exchanges in the Southwestern Atlantic Ocean: Numerical simulations. Journal of Geophysical Research: Oceans 119, 7949–7968.

Matano, R., Palma, E.D., Piola, A.R., 2010. The influence of the Brazil and Malvinas Currents on the Southwestern Atlantic Shelf circulation. Ocean Science 6, 983–995.

McDougall, T.J., Barker, P.M., 2011. Getting started with TEOS-10 and the Gibbs Seawater (GSW) oceanographic toolbox. Scor/Iapso WG 127, 1–28.

McGillicuddy Jr, D.J., 2015. Formation of intrathermocline lenses by eddy–wind interaction. Journal of Physical Oceanography 45, 606–612.

McGillicuddy Jr, D. J. (2016). Mechanisms of physical-biological-biogeochemical interaction at the oceanic mesoscale. Annual Review of Marine Science, *8*, 125-159.

Mill, G.N., da Costa, V.S., Lima, N.D., Gabioux, M., Guerra, L.A.A., Paiva, A.M., 2015. Northward migration of Cape São Tomé rings, Brazil. Continental Shelf Research 106, 27–37.

Möller Jr, O.O., Piola, A.R., Freitas, A.C., Campos, E.J., 2008. The eff ects of river discharge and seasonal winds on the shelf off southeastern South America. Continental shelf research 28, 1607–1624.

Müller, T.J., Ikeda, Y., Zangenberg, N., Nonato, L.V., 1998. Direct measurements of western boundary currents off Brazil between 20 S and 28 S. Journal of Geophysical Research: Oceans 103, 5429–5437.

Napolitano, D.C., Rocha, C.B., da Silveira, I.C., Simoes-Sousa, I.T., Flierl, G.R., 2021. Can the Intermediate Western Boundary Current recirculation trigger the Vitória Eddy formation? Ocean Dynamics 71, 281–292.

Palma, E.D., Matano, R.P., Piola, A.R., 2008. A numerical study of the Southwestern Atlantic Shelf circulation: Stratified ocean response to local and off shore forcing. Journal of Geophysical Research: Oceans 113.

Palóczy, A., Silveira, I.d., Castro, B., Calado, L., 2014. Coastal upwelling off Cape São Tomé (22 S, Brazil): The supporting role of deep ocean processes. Continental Shelf Research 89, 38-50.

Pascual, A., Ruiz, S., Buongiorno Nardelli, B., Guinehut, S., Iudicone, D., & Tintoré, J. (2015). Net primary production in the Gulf Stream sustained by quasi- geostrophic vertical exchanges. Geophysical Research Letters, 42(2), 441-449.

de Paula, T.P., Lima, J.A.M., Tanajura, C.A.S., Andrioni, M., Martins, R.P., Arruda, W.Z., 2021. The impact of ocean data assimilation on the simulation of mesoscale eddies at São Paulo plateau (Brazil) using the regional ocean modeling system. Ocean Modelling 0, 101889.

Pegliasco, C., Delepoulle, A., Mason, E., Morrow, R., Faugère, Y., Dibarboure, G., 2022. META3. 1exp: a new global mesoscale eddy trajectory atlas derived from altimetry. Earth System Science Data 14, 1087–1107.

Piola, A.R., Campos, E.J., Möller Jr, O.O., Charo, M., Martinez, C., 2000. Subtropical shelf front off eastern South America. Journal of Geophysical Research: Oceans 105, 6565–6578.

Piola, A.R., Matano, R.P., Palma, E.D., Möller Jr, O.O., Campos, E.J., 2005. The influence of the Plata River discharge on the western South Atlantic shelf. Geophysical Research Letters 32.

Piola, A.R., Palma, E.D., Bianchi, A.A., Castro, B.M., Dottori, M., Guerrero, R.A., Marrari, M., Matano, R.P., Möller, O.O., Saraceno, M., 2018. Physical oceanography of the SW Atlantic Shelf: a review. Plankton ecology of the Southwestern Atlantic: from the subtropical to the subantarctic realm , 37–56.

Rocha, C.B., Silveira, I.C.A.d., Castro, B.M., Lima, J.A.M., 2014. Vertical structure, energetics, and dynamics of the Brazil Current System at 22°S–28°S. Journal of Geophysical Research 119, 52–69. URL: http: //dx.doi.org/10.1002/2013JC009143, doi:10.1002/2013JC009143.

Rocha, C.B., Simoes-Sousa, I.T., 2022. Compact Mesoscale Eddies in the South Brazil Bight. Remote Sensing 14, 5781.

Rodrigues, M. L. G., Franco, D., Sugahara, S. 2004. Climatologia de frentes frias no litoral de Santa Catarina. Revista Brasileira de Geofísica, 22, 135-151.

Roughan, M., Keating, S. R., Schaeffer, A., Cetina Heredia, P., Rocha, C., Griffin, D., Robertson, R., Suthers, I. M., 2017. A tale of two eddies: The biophysical characteristics of two contrasting cyclonic eddies in the east australian current system. Journal of Geophysical Research: Oceans, *122*(3), 2494-2518.

Saraceno, M., Provost, C., 2012. On eddy polarity distribution in the southwestern Atlantic. Deep Sea Research Part I: Oceanographic Research Papers 69, 62–69.

Schmid, C., Majumder, S., 2018. Transport variability of the Brazil Current from observations and a data assimilation model. Ocean Science 14, 417–436.

Signorini, S.R., 1978. On the circulation and the volume transport of the Brazil Current between the Cape of São Tomé and Guanabara Bay. Deep Sea Research 25, 481–490.

Silveira, I.C., Bernardo, P.S., Lazaneo, C.Z., Amorim, J.P., Borges-Silva, M., Martins, R.C., Santos, D., Dottori, M., Belo, W.C., Martins, R.P., et al., 2022. Oceanographic conditions of the continental slope and deep Waters in Santos Basin: the SANSED cruise (winter 2019). Ocean and Coastal Research 71.

Silveira, I.C., Lima, J.A., Schmidt, A., Ceccopieri, W., Sartori, A., Francisco, C., Fontes, R., 2008. Is the meander growth in the Brazil Current system off Southeast Brazil due to baroclinic instability? Dynamics of Atmosphere and Oceans 45, 187–207.

Silveira, I.C., Pereira, F., Flierl, G.R., Simoes-Sousa, I.T., Palóczy, A., Borges-Silva, M., Rocha, C.B., 2023. The Brazil Current quasi-stationary unstable meanders at 22° S–23°S. Progress in Oceanography 210, 102925.

Soutelino, R., Da Silveira, I., Gangopadhyay, A., Miranda, J., 2011. Is the Brazil Current eddy-dominated to the north of 20 S? Geophysical Research Letters 38.

Stramma, L., England, M., 1999. On the water masses and mean circulation of the South Atlantic Ocean. Journal of Geophysical Research: Oceans 104, 20863–20883.

Szuts, Z., Blundell, J., Chidichimo, M., Marotzke, J., 2012. A vertical mode decomposition to investigate low-frequency internal motion across the Atlantic at 26 N. Ocean Science 8, 345–367.

Stech, J. L., Lorenzzetti, J. A. 1992. The response of the South Brazil Bight to the passage of wintertime cold fronts. Journal of Geophysical Research: Oceans, 97(C6), 9507-9520.

Suthers, I. M., Schaeffer, A., Archer, M., Roughan, M., Griffin, D. A., Chapman, C. C., Sloyan, B., Everett, J. D. 2023. Frontal eddies provide an oceanographic triad for favorable larval fish habitat. Limnology and Oceanography.

Uchoa, I., Simoes-Sousa, I.T., da Silveira, I.C., 2023. The Brazil Current mesoscale eddies: Altimetry-based characterization and tracking. Deep Sea Research Part I: Oceanographic Research Papers 192, 103947.

Valla, D., Piola, A. R., Meinen, C. S., & Campos, E. 2018. Strong mixing and recirculation in the northwestern Argentine Basin. Journal of Geophysical Research: Oceans, 123(7),4624-4648.

Visbeck, M., 2002. Deep velocity profiling using lowered acoustic Doppler current profilers: Bottom track and inverse solutions. Journal of Atmospheric and Oceanic Technology 19, 794–807.

Woodward, E., Rees, A., 2001. Nutrient distributions in an anticyclonic eddy in the northeast Atlantic Ocean, with reference to nanomolar ammonium concentrations. Deep Sea Research Part II: Topical Studies in Oceanography 48, 775–793.

Wunsch, C., 1997. The vertical partition of oceanic horizontal kinetic energy. Journal of Physical Oceanography 27, 1770–1794.

Zemba, J.C., 1991. The structure and transport of the Brazil Current between 27 and 36 south. Ph.D. thesis. PhD thesis, Woods Hole Oceanographic Institution, Woods Hole, MA, USA, 1991.

Zhang, H.M., Bates, J.J., Reynolds, R.W., 2006. Assessment of composite global sampling: Sea surface wind speed. Geophysical Research Letters 33.